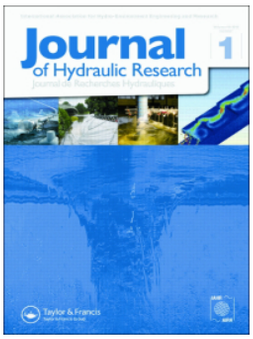

Journal of Hydraulic Research

ISSN: (Print) (Online) Journal homepage: www.tandfonline.com/journals/tjhr20

Benchmark of computational hydraulics models for open-channel flow with lateral cavities

Pablo Ouro, Luis Cea, Sergio Croquer, Wenhao Dong, Orlando Garcia-Feal, Adrián Navas-Montilla, Benedict D. Rogers, Tatsuhiko Uchida & Carmelo Juez

To cite this article: Pablo Ouro, Luis Cea, Sergio Croquer, Wenhao Dong, Orlando Garcia-Feal, Adrián Navas-Montilla, Benedict D. Rogers, Tatsuhiko Uchida & Carmelo Juez (2024) Benchmark of computational hydraulics models for open-channel flow with lateral cavities, Journal of Hydraulic Research, 62:5, 441-460, DOI: 10.1080/00221686.2024.2401905

To link to this article: https://doi.org/10.1080/00221686.2024.2401905

Published online: 17 Oct 2024.

JOURNAL OF HYDRAULIC RESEARCH
2024, VOL. 62, NO. 5, 441–460
https://doi.org/10.1080/00221686.2024.2401905

International Association for Hydro-Environment Engineering and Research
Hosted by Spain Water and IWHR, China
Taylor & Francis
Taylor & Francis Group

RESEARCH PAPER

Benchmark of computational hydraulics models for open-channel flow with lateral cavities

Pablo Ouro [a], Luis Cea [b], Sergio Croquer [c], Wenhao Dong[d], Orlando Garcia-Feal [b], Adrián Navas-Montilla [e], Benedict D. Rogers [a], Tatsuhiko Uchida [d] and Carmelo Juez [f]

[a]School of Engineering, The University of Manchester, Manchester, UK; [b]Water and Environmental Engineering Group, Center for Technological Innovation in Construction and Civil Engineering (CITEEC), Universidade da Coruña, A Coruña, Spain; [c]Département de Génie Mécanique, Université de Sherbrooke, Sherbrooke, Québec, Canada; [d]Graduate School of Advanced Science and Engineering, Hiroshima University, Hiroshima, Japan; [e]Fluid Dynamics Technologies, I3A-Universidad de Zaragoza, Zaragoza, Spain; [f]Consejo Superior de Investigaciones Científicas (IPE-CSIC), Instituto Pirenaico de Ecología, Zaragoza, Spain

ABSTRACT

Computational models in hydro-environmental engineering are diverse in their background formulation and span from two-dimensional depth-averaged shallow water models, to complex fully three-dimensional turbulence models resolving large-eddy simulation with surface capturing techniques, and to Lagrangian particle-based methods. This paper presents a first-of-its-kind comparison of six different computational hydraulics fluid dynamics models, namely Iber+, HO-SWM, GBVC, OpenFOAM (RANS), Hydro3D (LES) and DualSPHysics (SPH), in the prediction of mean velocities and free-surface dynamics in two benchmarks involving open-channel flows with symmetric lateral cavities. Results show that shallow-water models capture relatively well the main large-scale coherent structures of the in-cavity flow, with wider shear layers compared to three-dimensional models, and higher velocities in the main channel. Three-dimensional RANS, LES and SPH yield improved predictions of mean velocities compared with experimental data. Computational cost has been quantified for all models with a logarithmic growth when increasing model complexity. The transverse standing wave is captured by most models, with the shallow-water ones matching the theoretical value, while the three-dimensional models overestimate it slightly.

ARTICLE HISTORY
Received 20 November 2023
Accepted 3 September 2024
Open for discussion

KEYWORDS
Benchmark; computational hydraulics; large-eddy simulation; lateral cavities; Reynolds-averaged Navier–Stokes; shallow water model; SPH

1. Introduction

Computational hydraulics entails the use of computational fluid dynamics (CFD) for the resolution of water flows, an area in which a breadth of numerical tools have been developed over the last decades, and have proven to be very successful (Rodi, 2017; Sotiropoulos, 2015). The classic application of most of these models concerned open-channel and river flows, e.g. in application to flooding, compound channels or bed roughness turbulence. Newer applications are pushing the limits of computational hydraulics models involving, for instance, the forecast of extreme weather and flooding events (Cea, Álvarez et al., 2022; Guinot et al., 2017), scour protection (Khosronejad et al., 2012), sediment transport (Juez et al., 2022; Vowinckel et al., 2021; Zhao et al., 2023), or renewable energy generation devices (Juez & Navas-Montilla, 2022; Posa & Broglia, 2021), and are impacting positively on society (Sotiropoulos, 2019).

Free-surface effects, turbulence and transient flow phenomena are key unsteady flow features that need to be resolved or captured, at least to some extent, by models in computational hydraulics applications, in addition to the mean flow hydrodynamics, flow separation, recirculation, reattachment, etc. The relative importance of capturing each of these flow characteristics varies depending on the application or project at hand, as well as with the choice of the model given the flow physics that should be resolved (Constantinescu, 2006; Rodi et al., 2013). Performing benchmarks comparing different numerical approaches provides new insights into their actual capabilities and trade-off between computational expense and simulated flow physics, which informs researchers, industry and policy makers. This is the motivation for this first international computational hydraulics benchmark applied to open-channel flows.

In shallow flow conditions, when the water depth is multiple times smaller than the channel width, the flow becomes mostly two-dimensional (2-D) with large-scale coherent structures carrying most of the kinetic energy (Uijttewaal, 2019). A particularly interesting aspect of some shallow hydraulic flow is the inverse turbulent cascade, sometimes referred to as backscatter, in which relatively small flow scales can lead to the generation of quasi-2-D eddies. This concept is

CONTACT Pablo Ouro pablo.ouro@manchester.ac.uk

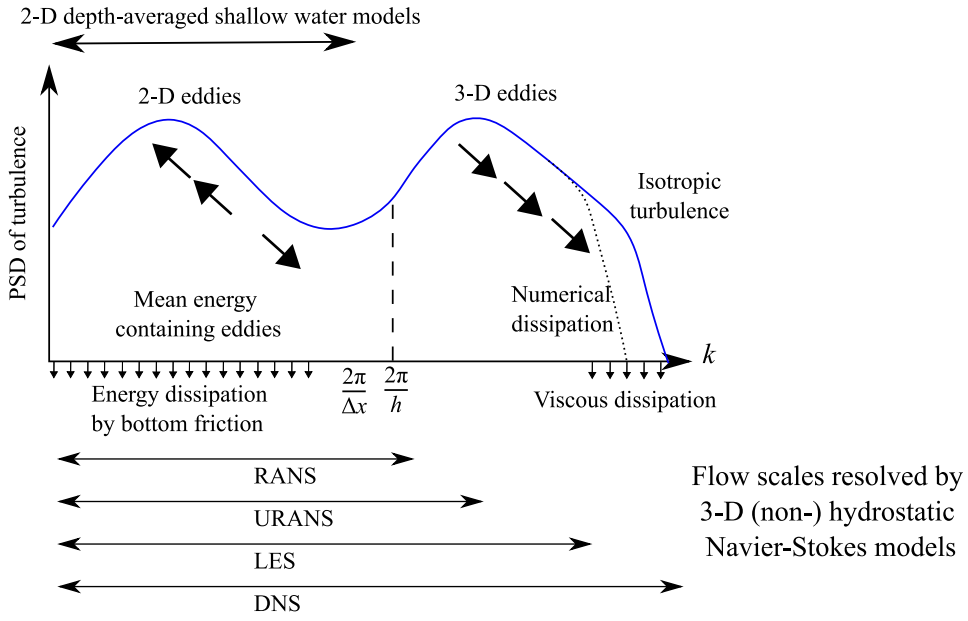

Figure 1. Power spectral density distribution of turbulence in shallow flows, characterized by the presence of an inverse turbulence cascade when 2-D eddies are generated from the energy transfer of smaller scales. Adapted from Nadaoka and Yagi (1998).

summarized in Figure 1, adapted from the work from Nadaoka and Yagi (1998). Conversely, when the flow is purely three-dimensional, the classic turbulence decay spectrum is developed with the production, inertial and dissipation ranges (Rodi et al., 2013).

One of the reasons for the success of computational hydraulics models applied to river hydraulics and open channel flows is the good performance of the Saint-Venant equations, also referred to as the shallow water equations (SWEs), which assume a hydrostatic pressure distribution to yield the well-known two-dimensional depth-averaged shallow-water models (2-D-SWM). Their main advantages are the flexibility and adaptability to model complex physical scenarios (e.g. irregular bathymetry, wet–dry fronts, time-varying inflow conditions) and their balance between accuracy and computational efficiency. The 2-D-SWMs can incorporate the turbulent effects derived from the bottom friction and horizontal shear by means of explicit turbulence models, e.g. the mixing-length or depth-averaged $k - \varepsilon$; see Rastogi and Rodi (1978) models or Cea et al. (2007) for extensive reviews. Furthermore, some depth-integrated models have been developed to resolve the vertical distribution of velocity and pressure (Uchida & Fukuoka, 2014), as well as to include in some way non-hydrostatic effects (Castro-Orgaz et al., 2023; Gamero et al., 2022; Wang et al., 2020) or the possibility of modelling vertically confined flows (Cea & López-Núñez, 2021; Maranzoni et al., 2015). Recent work on 2-D-SWMs has also focused on improving their computational efficiency by implementing high-performance computational techniques, either on multiple CPUs or taking advantage of graphics processing units (GPUs) (García-Feal et al., 2018; Morales-Hernández et al., 2020; Sanders & Schubert, 2019; Xia et al., 2019), developing subgrid parameterizations to account for small scale features not resolved by the computational mesh (Dewals et al., 2021; Henonin et al., 2015; Sanders & Schubert, 2019; Shamkhalchian & De Almeida, 2021), and implementing internal conditions to account for the effect of hydraulic structures such as bridges or weirs (Cea, Vila, et al., 2022; Dazzi et al., 2020; Kalita et al., 2019; Lacasta et al., 2018).

Three-dimensional (3-D) shallow-water models also assume a hydrostatic pressure distribution and make use of multiple layers to account for 3-D flow structures or bottom friction. 3-D non-hydrostatic models are becoming more used in practical hydro-environmental applications, mainly due to the increase in computational capacity, often solved using multi-node multicore machines with parallelization protocols such as MPI, OpenMP, or OpenACC, or combinations of those (Ouro et al., 2019), or even GPUs (Sweet et al., 2018). They are computationally expensive mainly due to the need for iteratively resolving the Poisson pressure equation, but enable a high resolution of the turbulent flow field. The main turbulence closures used in 3-D models are Reynolds-averaged Navier–Stokes (RANS) and large-eddy simulation (LES), with direct numerical simulations still restricted to relatively low Reynolds numbers due to the extreme computational expense (Sotiropoulos, 2015; Stoesser, 2014). Hybrid turbulence models such as detached eddy simulation (DES) or partially averaged Navier–Stokes (PANS) offer an improved computational balanced mainly due to a smaller number of grid cells required (Guillén Ludeña et al., 2017).

Whilst most computational hydraulics models are Eulerian (fixed grid-based) methods, there is a growing

Table 1. Flow physics captured, modelled or resolved by the different numerical schemes and associated order of magnitude of their computational cost.

Numerical framework	Turbulence closure	Free-surface boundary	Turbulence	Free-surface effects	Transient phenomena	computational cost
1st–2nd order SWM	Depth-averaged RANS	Hydrostatic	Modelled	Yes	No	10^1 CPU h
High-order SWM	Depth-averaged RANS	Hydrostatic	Modelled	Yes	2-D large-scales	10^2 CPU h
	RANS	Rigid-lid	Modelled	No	No	10^3 CPU h
	URANS	Rigid-lid	Modelled	No	Large scales	10^4 CPU h
3-D Navier–Stokes	URANS	Hydrostatic	Modelled	Yes	Large scales	10^5 CPU h
	LES	Rigid-lid	Resolved	No	Yes	10^5 CPU h
	LES	Hydrostatic	Resolved	Yes	Yes	10^6 CPU h
Lagrangian particles	Sub-particle	Dynamic	Modelled	Yes	Large scales	GPU

applicability and use of particle-based methods in hydrostatic 2-D and 3-D simulation frameworks, which adopt individual Lagrangian markers that are advected as a result of the forces driving the flow (Dalrymple & Rogers, 2006; Domínguez et al., 2022). Smoothed-particle hydrodynamics is one of the most successful Lagrangian methods in computational hydraulics (Violeau & Rogers, 2016); thanks to its maturity it was implemented in a wide range of applications (Gotoh & Khayyer, 2018; Manenti et al., 2019; Shadloo et al., 2016). Their main advantage lies in the ability to resolve complex, violent free-surface flows without needing to generate a computational grid (Violeau & Rogers, 2016). Despite their high computational cost, these methods have benefited from the computational capabilities of GPUs, making it possible to solve problems with millions of particles in reasonable times. Many examples of GPU accelerated SPH solvers can be found in the literature (Cercos-Pita, 2015; Domínguez et al., 2022; Hérault et al., 2010; Park et al., 2020).

The capabilities in predicting flow phenomena of the various computational hydraulics models analysed in this work are summarized in Table 1, and are classified as: 2-D shallow-water models, Eulerian 3-D incompressible Navier–Stokes and (quasi-incompressible) Lagrangian particle methods. These further sub-divisions depend on their spatial discretization order of accuracy and/or their free-surface treatment. Three main aspects of their capability to predict hydro-environmental fluid flows are turbulence, transient phenomena (coherent large-scale structures) and free-surface effects. An indication of the computational cost of each model is provided in terms of CPU hours, albeit comparison with GPU-computed models can be tricky. This is justified in this paper with computational expenses from the different models used. We note other advanced computational methods are being developed for hydraulics, such as lattice Boltzmann, but are less widely used to date.

This paper provides a first-of-its-kind extensive cross-comparison between various numerical computational hydraulics models involving codes of distinct capabilities and underlying physics. It addresses questions about:

- what are the advantages of adopting either a three-dimensional turbulence resolving model or a two-dimensional steady model?
- what are the computational cost associated to those codes for the same simulation setup?
- is it more important to resolve the three-dimensional velocity field or capturing free-surface effects and two-dimensional flow field?

This benchmark is intended to provide answers to these questions, motivating the computational hydraulics community to perform similar projects to inform the academic and industrial communities when carrying out complex numerical simulations.

Although many flows in river hydraulics can be characterized as open-channel flows (e.g. flows in rivers, harbours, estuaries), this benchmark exercise focuses on two open-channel flows featuring periodic symmetric lateral cavities. These experimental tests were selected due to the developed complex flow hydrodynamics, including presence of free-surface standing waves due to resonance effects or coherent turbulent structures dominating the shear layers over the openings of the cavities. Such flows have been studied extensively, experimentally and numerically (see for instance: Barros & Escauriaza, 2024; Engelen et al., 2021; Juez, Buhlmann, et al., 2018; Mignot et al., 2016; Ouro et al., 2020a, 2020b), but remain yet to be fully understood as flow three-dimensionality and coupling between resonant effects and vortex shedding vary with bulk flow conditions and cavity geometry. Here, six computational hydraulics models have been considered; short descriptions are presented in Table 2.

The description of the experimental setup is provided in Section 2, with an explanation of the six models provided in Section 3. In Section 4, results are compared in terms of velocity distribution across selected transverse and longitudinal profiles within a selected lateral cavity from which experimental data is available. Another goal of this paper is to provide an open discussion of the ability of each model to capture different governing flow structures, balanced with their computational expense, which is provided in Section 5 together with some lessons learnt during this benchmark.

Table 2. Computational hydraulics models used in the present review. Note that the simpleFOAM version of OpenFOAM is adopted.

Code Name	Numerical framework	Free-surface boundary	Details
Iber+	2nd order SWM	Hydrostatic	2-D-SWM with Godunov-type schemes that runs on CPUs and GPUs.
BVC	2nd order SWM	Hydrostatic	Method to resolve depth-scale 3D vortex motions with depth-averaged equations.
HO-SWM	High-order SWM	Hydrostatic	2-D-SWM with high-order WENO schemes.
OpenFOAM	3-D Navier–Stokes	Rigid-lid	3-D finite-volume solver with URANS $k-\varepsilon$ and $k-\omega$ SST turbulence closures.
Hydro3D	3-D Navier– Stokes	Rigid-lid	3-D finite-difference solver with LES turbulence approach.
DualSPHysics	SPH	Dynamic	3-D Lagrangian particle model with sub-particle turbulence scheme.

2. Description of the benchmarks

Two open-channel flow experiments with symmetric lateral cavities on the channel sides are used as benchmark cases. These experiments were carried out in a channel which works in a closed circuit. The experimental flume was 7.5 m long, 1.0 m wide and 0.5 m high. The longitudinal slope of the channel is 0.1%. The channel bottom is smooth and made of painted wood. The walls of the channel are made of glass. Downstream from the channel, a Venetian gate allows the flow depth to be controlled. The hydrodynamic response of these experiments was assessed by means of velocity (surface particle image velocimetry (PIV)) and water surface elevation (ultrasounds probes) measurements. More details can be found in Juez, Buhlmann, et al. (2018) and Juez, Thalmann, et al. (2018).

2.1. Benchmark 1

The first benchmark is based on the geometric configuration 2.1 tested in Juez, Buhlmann, et al. (2018) and presented in Figure 2. This geometric configuration is characterized by a total width of the channel $B = 1.0$ m, a width of the base channel $b = 0.6$ m, a length of the cavities equal to $l = 0.25$ m, a cavity width $w = 0.20$ m, and a separation between cavities of $L = 0.5$ m. The flow was imposed to have uniform inflow conditions with a $Q = 8.5\,\mathrm{l\,s^{-1}}$ and $h = 0.048$ m at the outlet. Reynolds number was above 50,000 and Froude number was equal to 0.421. The cavity in which surface PIV measurements were taken is highlighted in red and experimental measurement of water depth was done at the location of probes P1, P2 and P3 (Figure 2). The central cavity to record PIV measurements was chosen because it is representative of the flow patterns for all the other cavities. This cavity is away from perturbing effects from the upstream and downstream channel boundaries.

2.2. Benchmark 2

The second benchmark is based on the geometric configuration 3.1 tested in Juez, Buhlmann, et al. (2018) and shown in Figure 3. This geometric configuration is characterized by a total channel width of $B = 1$ m, a base channel width of $b = 0.5$ m, a cavity width $w = 0.20$ m, and a length of the cavities equal to their separation, that is $l = L = 0.5$ m. Reynolds number was above 58,000 and Froude number was equal to 0.504. The cavity in which surface PIV measurements were taken is highlighted in red and experimental measurement of water depth was done at the location of probes P1, P2 and P3 (Figure 3). Criteria for selecting this cavity is analogous to the previous benchmark. The flow was configured to be uniform, with $h = 0.05$ m and $Q = 8.5\,\mathrm{l\,s^{-1}}$. In this particular configuration, an in-cavity transversal seiche was reported with a period of $T = 2.84$ s (Juez, Buhlmann, et al., 2018).

2.3. Cavity flow overview

For each of the benchmarks, every participant was asked to extract time-averaged velocity data over six profiles, three in the flow direction within the cavity at $y/w = 0.4, 0.6$ and 0.8, and transverse to the main flow at $x/l = 0.25, 0.50$ and 0.75, with the origin of coordinates at the bottom left of a selected cavity (see Figure 4). The location of these profiles provides details of the main flow features expected to be developed within such cavities, namely: a single-core recirculation vortex; a shear layer at the cavity mouth over which coherent Kelvin–Helmholtz structures travel downstream and hit the downstream wall; and a possible transverse standing wave triggered by the natural resonant frequency of the channel with symmetric lateral cavities.

3. Description of the computational hydraulics codes

This section presents a brief description of the six computational models compared in the two benchmarks, including the underlying physics, numerical discretization, parallelization type (if any), domain size, mesh typology and boundary conditions. For simplicity, the notation in the models' description is independent.

3.1. Iber+

Iber+ (García-Feal et al., 2018) is a high-performance computing (HPC) implementation of the software Iber (Bladé et al., 2014), which solves the two-dimensional (2-D) shallow water equations (2-D-SWE) including several depth-averaged eddy viscosity turbulence models (Cea et al., 2007). The solver is parallelized for

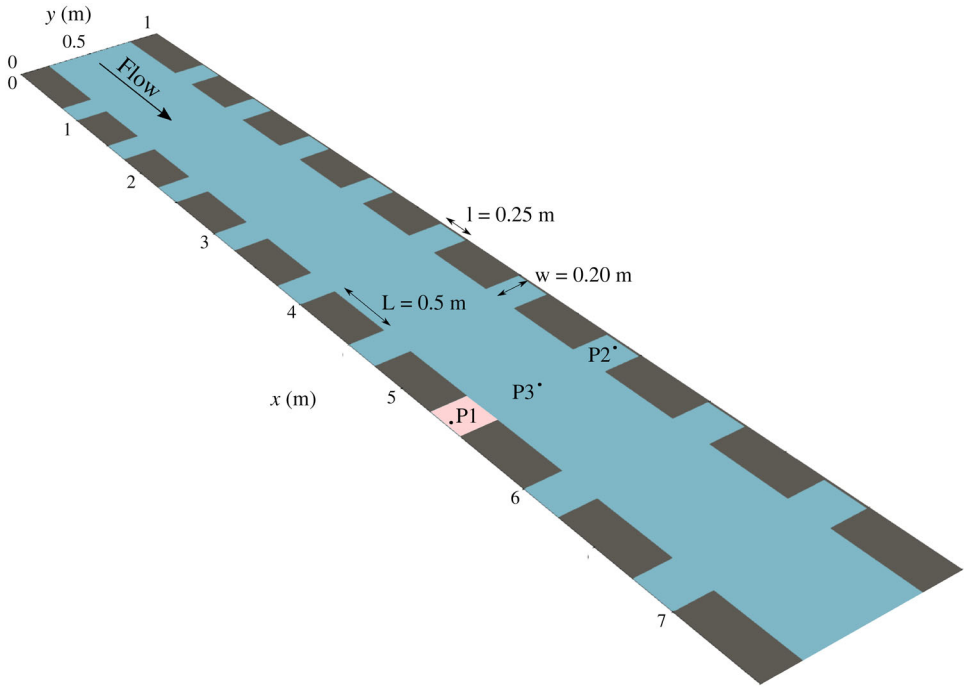

Figure 2. Schematic of the experimental geometric configuration 2.1 (Benchmark 1) including the relevant dimensions. The cavity in which PIV measurements were taken is highlighted in red. P1, P2 and P3 indicate location of probes from which time series of velocities are taken.

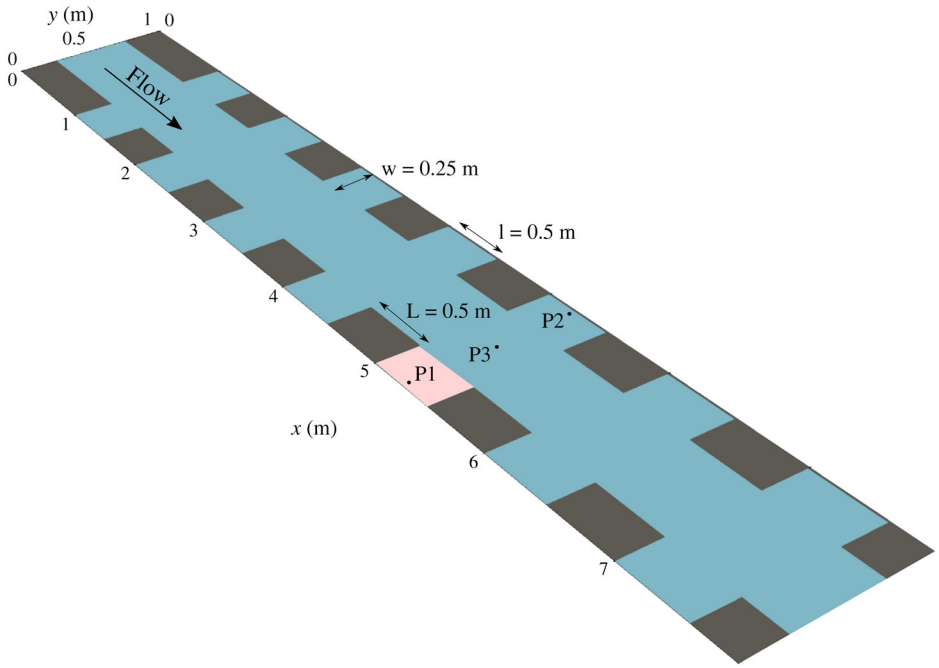

Figure 3. Schematic of the experimental geometric configuration 3.1 (Benchmark 2) including the relevant dimensions. The cavity in which PIV measurements were taken is highlighted in red. P1, P2 and P3 indicate location of probes from which time series of velocities and free-surface elevation are taken.

CPU using OpenMP, and for GPU using Nvidia CUDA. The GPU implementation, which is the one adopted in this study, can achieve speed-ups of two orders of magnitude when compared with the non-parallelized version (García-Feal et al., 2018). The software is freely available at www.iberaula.com.

Iber was initially developed to model flow in rivers and open channels, and it was later on extended to model overland flow at the catchment scale including rainfall and infiltration source terms (Cea & Bladé, 2015). The eddy viscosity can be computed using three depth-averaged eddy viscosity turbulence models (Cea et al., 2007), namely parabolic profile, mixing length, and the $k - \varepsilon$ model of Rastogi and Rodi (1978). The later one was the one used in all the simulations presented in this study.

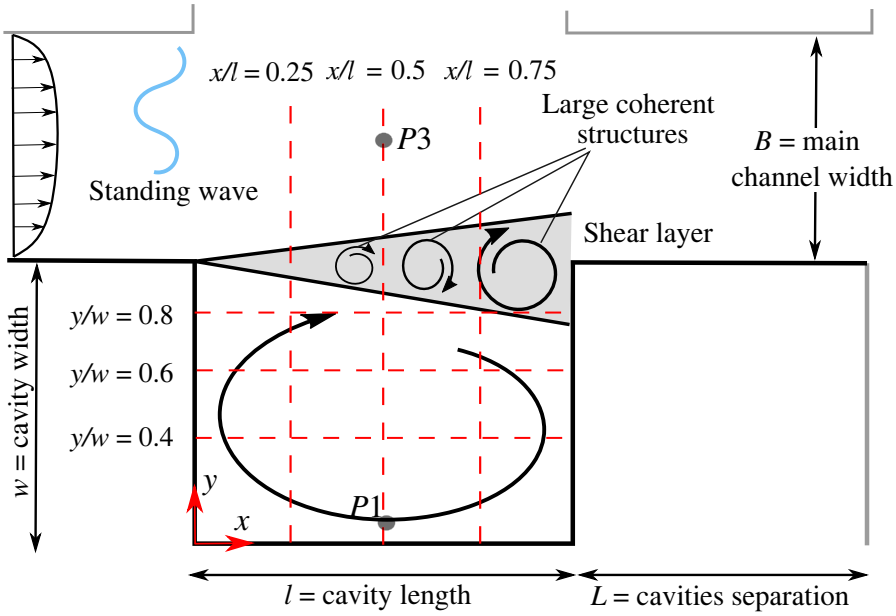

Figure 4. Sketch of the main flow features developed from the interaction of a lateral cavity and main channel, highlighting the location of the longitudinal (*x*-direction) and transverse (*y*-direction) profiles at selected local *y*/*w* and *x*/*l*. Adapted from Ouro et al. (2020a).

The 2D-SWE are solved with an explicit unstructured finite volume solver, although the meshing algorithm allows the user to create structured grids made of quadrilaterals or unstructured grids made of irregular triangles. The solver includes several schemes for the discretization of the convective fluxes. A Godunov type scheme based on Roe's approximate Riemann solver (Toro, 2001) was used in all the simulations performed in this work. Bed-friction is discretized with a semi-implicit scheme to enhance the numerical stability of the solver for very shallow flows. Mathematical details about the discretization schemes implemented in the model can be found in several previous publications (Cea & Vázquez-Cendón, 2012).

Description of the numerical setup

The experimental geometry of the flume was replicated in the numerical model, i.e. a 7.5 m long and 1.0 m wide flume, with a longitudinal slope of 0.1%, including 2 × 9 cavities in benchmark 1 and 2 × 7 cavities in benchmark 2. A Manning roughness coefficient of 0.012 was assumed for the bed as well as for the lateral closed boundaries. At the outlet boundary a water depth of 0.048 and 0.050 m was imposed in benchmarks 1 and 2 respectively, while a total inlet discharge of 8.5 l s^{-1} was imposed at the upstream boundary in both cases.

Two different spatial discretizations were tested: a structured grid made of uniform quadrilaterals of 0.01 m length, and an unstructured grid made of triangles with an average side of 0.01 m. The total number of mesh elements was 54,000 and 123,066 for the structured and unstructured meshes respectively. With this mesh configuration, each individual cavity was discretized with 500 and 1116 elements in the structured and unstructured grids.

A CFL condition equal to 0.45 was used, which, for the flow conditions and numerical grids used produced a computational time step of roughly 0.0045 s and 0.0025 s in benchmark 1 for the structured and unstructured grids, respectively. The total simulation time was 300 s in both cases, although after 100 s a steady state was achieved in the whole channel.

3.2. HO-SWM

The high-order shallow-water model (HO-SWM) is a two-dimensional URANS shallow water model, which accounts for bed topography, friction and turbulent mixing (Navas-Montilla et al., 2019). It has been validated in challenging free-surface shallow flows involving standing waves and turbulence (Juez & Navas-Montilla, 2022; Navas-Montilla et al., 2019, 2021). The model is able to resolve the large-scale coherent horizontal vortices, while capturing transient water surface fluctuation phenomena. Small scale turbulence is not resolved but its contribution to the mean flow is considered by means of an algebraic turbulence model. The HO-SWM is composed of the depth-averaged equations for the conservation of mass and momentum in *x*- and *y*-directions. Friction and bed slope source terms are considered in the momentum equations. The friction coefficient is computed by means of Manning's formulation. To account for the effect of the unresolved turbulent motion, the depth-averaged turbulent stresses are approached using the Boussinesq approximation. The eddy viscosity is

computed using the depth-averaged mixing length model.

A 3rd–order finite-volume WENO-ADER scheme is used for the numerical discretization of the equations, in combination with an augmented Roe solver to compute the numerical fluxes (Navas-Montilla et al., 2019). This method features a high order of accuracy in smooth regions, while capturing sharp gradients in under-resolved regions of the flow, without spurious oscillations. The HO-SWM adopts an URANS framework that allows to resolve large-scale 2-D horizontal vortices while small-scale 3-D turbulence is modelled. At the same time, gravity waves are accurately captured as a result of the shock-capturing properties of the solver. This makes the HO-SWM a good candidate for the resolution of the benchmark cases herein considered, which involve capturing phenomena coupling gravity waves and turbulence.

Description of the numerical setup

The computational domain considers the experimental dimensions with a 7.5 m long and 1.0 m wide flume, a longitudinal slope of 0.1%, and with 2 × 9 cavities in benchmark 1 and 2 × 7 cavities in benchmark 2. A Manning roughness coefficient of 0.01 is considered for the bed and glass walls, whereas a roughness coefficient of 0.03 is considered for the brick walls. At the outlet boundary, a water depth of 0.050 m is imposed, while an inlet discharge of 8.5 l s^{-1} is set at the upstream boundary in both benchmarks. The algebraic mixing length turbulence model is configured setting the empirical coefficient $\lambda = 0.16$ for the vertical component of the turbulent viscosity due to bed shear and the calibration constant $\beta = 0.05$ adopted to compute the horizontal component of the turbulenct viscosity, analogously to Navas-Montilla et al. (2019).

The spatial domain is discretized using uniform square grid cells with $\Delta x = 0.005$ m. In benchmark 1, the number of elements is 310,000, whereas the grid in benchmark 2 is comprised of 340,000 elements. The integration in time is done using a variable time step setting a CFL condition equal to 0.45. The total simulation time is 300 s and mean velocities are computed after 240 s, when a uniform seiche oscillation is observed. The simulations were run on a single CPU with 24 OMP threads during 48 h.

3.3. Bottom velocity computation (BVC) method

The bottom velocity computation (BVC) method is a quasi-3-D depth-integrated RANS model, which can calculate the third (vertical) velocity component and horizontal velocity components in the third dimension (Uchida & Fukuoka, 2019; Uchida et al., 2016). It assumes the vertical profiles of the horizontal velocity components in x_i direction follow a cubic function that reads:

Table 3. Governing equations for the set of BVC models.

Unknown variables	Governing equations	2DC	SBVC	GBVC
Water depth h	DI continuity	✓	✓	✓
DA horizontal velocity U_i	DI horizontal momentum	✓	✓	✓
Kinetic energy k	DI kinetic turbulence energy	✓	✓	✓
Horizontal bottom velocity u_{bi}	DI definition equations of horizontal velocity	–	✓	✓
DA horizontal vorticity Ω_i	DI horizontal vorticity	–	✓	✓
Horizontal water surface velocity u_{si}	Horizontal momentum equations on water surface	–	✓	✓
Vertical velocity W	Double integrated continuity	–	–	✓
Bottom pressure deviation d_{pb}	DI vertical momentum	–	–	✓

$$u_i = (u_{si} - U_i)(12\eta^3 - 12\eta^2 + 1) + (u_{si} - u_{bi})(-4\eta^3 + 3\eta^2) + U_i \quad (1)$$

where u_i is the velocity at elevation z; u_{si} is the water surface velocity; U_i is the depth-averaged velocity; $\eta = (z_s - z)/h$, z_s is the water surface elevation, h is the water depth; u_{bi} is the bottom velocity. One of the important roles of the vertical velocity distribution of Equation (1) is to evaluate the horizontal shear stress term in the horizontal momentum, which allows the model to resolve depth-scale 3-D vortex motions and consider the energy cascade process (Figure 1) within a two-dimensional calculation framework.

The governing equations of the BVC method are derived from a three-dimensional RANS model as shown in Table 3, using the vertical velocity profile of Equation (1). A set of depth-integrated equations are solved to calculate unknown variables in Equation (1). The BVC model can be comprised of three different methods: (i) a conventional two-dimensional computational (2DC) model to solve the shallow water without considering non-equilibrium velocity and pressure distribution in the vertical direction; (ii) a simplified bottom velocity computation (SBVC) model employing depth-integrated vorticity equations in horizontal directions and horizontal momentum equation on water surface to calculate non-equilibrium velocity distribution of Equation (1); and (iii) a general bottom velocity computation (GBVC) model advanced by depth-integrated momentum equation in the vertical direction for non-hydrostatic pressure component and double integrated continuity equation for the depth-averaged vertical velocity.

In the numerical procedure, the advection term of the depth-integrated momentum equation is discretized by the constrained interpolation profile (CIP)

scheme with third-order accuracy, and the other terms in the governing equations are discretized by the central differencing scheme with second-order accuracy. Except for the bottom flow velocity equation for u_{bi} and the equations related to the GBVC method, the basic equations in Table 3 are solved by the first-order accurate forward difference method for the local acceleration term with a fixed time interval. The bottom velocity equation and the vertical velocity equation for GBVC method are coupled and solved implicitly by deriving Poisson-type equations (Uchida & Fukuoka, 2014). For the eddy viscosity coefficient ν_t, a one-equation turbulence model is employed.

Description of the numerical setup

The computational domain is set according to the actual experimental geometry, which is an open-channel facility of 7.5 m length and 1.0 m width with a slope of 1/1000. A Manning roughness coefficient of 0.009 is assumed for the channel bed. The hydraulic conditions are set consistently with the experimental conditions indicated in Section 2. The boundary conditions are established with a fixed flow rate at the upstream end and constant water level at the downstream end. The bottom shear stress is evaluated by an equivalent roughness $k_s = 0.1$ mm. The computational grid is uniform with $\Delta x = \Delta y = 0.01$ m, yielding a total number of cells of 75,851. The total simulation time is 600 s and CPU hours are equal to 75 h for GBVC using a single AMD EPYC 7713 64-core Processor, which is 1.5 times longer than the 2DC code (52 h).

3.4. OpenFOAM

OpenFOAM is a free open-source C++ toolbox specialized for computational fluid dynamics. It provides a variety of object classes allowing the manipulation of fields, geometries and discretization techniques (Darwish & Moukalled, 2016), including over 100 solvers based on the finite volume method. In this method, the flow field is obtained by dividing the computational domain into discrete cells, and solving a the discretized governing equations in their conservative form at each of these cells. Field variables (such as pressure, velocity, turbulent kinetic energy, etc) are stored at the cells' centroids, while the fluxes of these variables are computed at each cell face using a selection of interpolation schemes. The flow is modelled using the 3D incompressible RANS solver *simpleFoam* for steady state single-phase (no air, no air–water interface), with the steady-state scheme for temporal discretization, the Gauss limitedLinear scheme for spatial divergence terms in the velocity and stress equations, and the upwind scheme for the divergence terms in the turbulence equations. In addition, two different turbulence models were assessed for each solver: the standard $k-\varepsilon$ (Launder & Sharma, 1974) and $k-\omega$ SST (stress shear transport) model (Menter, 1994).

Description of the numerical setup

The computational domain includes two cavities on the same side with a symmetry condition along mid-plane of the main channel adopted. The main channel extends over a distance of 0.25 m before and after the cavities. The domain height was set equal to $h = 0.05$ m and a uniform grid topology with hexahedral elements of $\Delta x = 0.003$ m, $\Delta y = 0.003$ m and $\Delta z = 0.004$ m is used in all cases. The meshes had 1.2 million grid cells. The element size is chosen based on a grid independence test done for Benchmark 1. Regarding time discretization, a fixed time step $\Delta t = 0.01$ s was prescribed based on preliminary calculations to assess the model's stability.

As per the boundary conditions, inlet-outlet conditions are set to translational periodicity with an adaptive momentum source which adjusted the outlet-inlet pressure gradient to ensure a prescribed mean velocity. The constant prescribed mean inlet velocity was set accordingly to the experimental flow conditions. A no-slip condition was set at the lateral walls and the flume bottom, with standard wall functions for the turbulent quantities: k, ε and ω. The mean normalized wall distance (z^+) varied between 10 and 60, depending on the benchmark. At the top of the domain a slip wall is adopted.

All cases were initialized using a prescribed velocity and surface height level at the inlet considering the reference benchmark data from experiments. The converged flow field is then used as the initial condition for the following run adopting inflow-outflow periodicity in the streamwise direction. Steady state cases are run for a simulated time of 15,000 s whilst transient cases are run for a simulated time of at least 2000 s. Results are averaged once pressure and turbulence residuals were lower than 10^{-4} and velocities in the cavity stabilized, i.e. they varied less than 1% during the last 500 iterations. The simulated time was 3000 s. All computations were performed on the Niagara supercomputer at the SciNet HPC Consortium (Loken et al., 2010; Ponce et al., 2019). Each case was run on 120 CPUs Intel 'Skylake' at 2.4 GHz distributed across four nodes, each with 202 Gb RAM. Approximated computational time was two days for steady state cases (simpleFoam).

3.5. Hydro3D

Hydro3D is an in-house code using LES based on finite differences to resolves the governing equations on rectangular Cartesian grids with staggered storage of velocities (Ouro et al., 2019, 2021). Hydro3D has been well validated in challenging turbulent environmental flows in the field of hydraulics (Stoesser, 2010), lateral bank cavities (Ouro et al., 2020a, 2022), or rough beds (Bomminayuni & Stoesser, 2011), among other engineering applications. The code resolves the spatially filtered Navier–Stokes equations with sub-grid-scale

stresses computed using the wall-adapting local eddy-viscosity (WALE) sub-grid scale model. To advance the simulation in time, a predictor-corrector fractional step method is employed with a three-step low-storage Runge–Kutta scheme and a multi-grid pressure solver. In the present benchmarks, second-order central differences are employed for the diffusive terms while a 5th-order weighted essentially non-oscillatory (WENO) scheme is adopted to compute the convective fluxes. Domain decomposition is used to parallelize the computational domain into identical sub-domains whose communication is performed using the standard message passing interface (MPI) to enable the exploitation of HPC. Hydro3D is characterized by its adaptability to resolve hydro-environmental free-surface flows, static and dynamic solid bodies, transport of Lagrangian particles and passive scalars, sediment particles, etc.

Description of the numerical setup

Lateral cavities in open-channel flows are simulated in Hydro3D with two approaches. Firstly, the entire experimental flume is simulated with inflow-outflow conditions with a constant flow discharge imposed at the inlet with a uniform velocity distribution. Alternatively, another simulation setup considered a shorter streamwise domain featuring two lateral cavities on each side of the open channel with periodic streamwise boundary conditions driven by a pressure gradient that keeps the mass flow rate constant, i.e. representing an infinitely long flume. The advantage of reducing the streamwise domain is that the LES is carried out with 100 CPUs whilst the entire domain simulation setup requires 600 CPUs. However, results have shown that the periodic boundary conditions in the main channel can induce a fully developed flow conditions which might not represent the flow development found at the measured cavity with PIV in the experiments (Figure 2), e.g. there could be secondary flow and a larger near-wall boundary layer development. In the following, we present the results with the entire flume simulation and vertically-averaged velocity values to allow comparison with the depth-averaged shallow-water models.

No-slip conditions are set at the bottom surface and flume and cavity walls as the grid resolution is fine enough to have the first cell off-the-wall in the viscous sub-layer (Ouro et al., 2020a). A shear-free rigid lid condition is adopted at the free surface and hence free-surface effects cannot be explicitly captured. The time step is variable with a CFL condition equal to 0.3. As LES resolves the unsteady turbulent flow structures, the mean velocities are computed after 30 s from the start of the simulation to discard initial transients, and 170 s after second order statistics start to be averaged, with the total simulation time equal to 330 s. The mesh comprises 300 million grid elements which run on 600 Intel Skylake Xeon 6148 Gold CPUs on Supercomputing Wales.

3.6. DualSPHysics

DualSPHysics is an open-source smoothed particle hydrodynamics (SPH) solver developed by the Universidade de Vigo (Spain), University of Manchester (UK), Università degli studi di Parma (Italy), Universitat de Politecnica de Catalunya, Barcelona Tech (Spain) and New Jersey Institute of Technology (USA). DualSPHysics solves the weakly compressible form of the Navier–Stokes equations for conservation of mass and momentum in Lagrangian form. The weakly compressible assumption allows use of an equation of state with a speed of sound that keeps density variations within 1% which is acceptable for engineering applications and enables simulations to be completed within a reasonable runtimes. For the Navier–Stokes equations, SPH enables a fully Lagrangian 3D simulation of the hydrodynamics providing velocities, densities, pressure and other flow properties for the moving particles (Violeau & Rogers, 2016), making it ideally suited to investigating fundamental physical processes and their application in fluid dynamics (Shadloo et al., 2016). The DualSPHysics code is designed to exploit the hardware acceleration provided by graphics processing units (GPUs), specifically Nvidia GPUs and the CUDA programming framework. This enables simulations with 100 million particles to be run on a single GPU. First released in 2011, the latest version of the code includes multiple formulation for viscosity, improved boundary conditions, and fluid–structure interaction exploiting the use of libraries to extend its application to a wide range of free-surface flows. To limit fluctuations in the density and pressure fields, density diffusion techniques (Fourtakas et al., 2019) have been employed in the DualSPHysics simulations presented herein. To take account of turbulence, the weakly compressible sub-particle scale (SPS) LES formulation developed by Rogers and Dalrymple (2005) and Dalrymple and Rogers (2006) is used. For the inflow-outflow conditions boundary conditions, the simulations make use of the functionality introduced by Tafuni et al. (2018). A full description of the DualSPHysics code and the formulation is found in Domínguez et al. (2022).

Description of the benchmark numerical setup

The full numerical flume as shown in Figures 2 and 3 is modelled with DualSPHysics. The flow is driven by imposing the inflow-outflow boundary conditions as indicated above along with changing the gravity vector to represent the gradient of the channel. No-slip boundary conditions are used on all solid boundaries. The initial interparticle distance, $dp = 0.005$ m giving approximately 3 million particles. The Wendland smoothing kernel is used with a ratio of smoothing length h to dp of 2. Symplectic timestepping is used with a CFL number of 0.2. Density diffusion is activated without particle shifting (Fourtakas et al., 2019). Simulations

are started with a uniform velocity equal to the average inflow velocity for each configuration. Simulations have been run using an NVIDIA RTX3060 GPU that has 3584 threads.

4. Results

This section presents the comparison of the time-averaged velocity field computed for the two benchmarks by the six numerical models, together with the analysis of the time series of water depth or pressure fluctuation (codes that used a rigid-lid approach) at selected locations for benchmark 2 in which a standing wave occurred during the experiments (not present for benchmark 1 setup). Results from OpenFOAM and BVC method are those considering the $k-\omega$ SST turbulence model and GBVC respectively unless otherwise stated. Velocity results Hydro3D and DualSPHysics are depth-averaged. Details of the computational cost relative to number of grid cells and computational resources are provided at the end of this section to provide a quantification that balances the computational expense of each model to the resolved physics.

4.1. Benchmark 1

A quantitative comparison between models is presented in Figures 5 and 6 containing transverse and longitudinal profiles at $y/w = 0.40, 0.60$ and 0.80 of time-averaged streamwise (U) and transverse (V) velocities at selected locations shown in Figure 4. In the profiles at $y/w = 0.40$, shown in Figure 5a, all models agree with the PIV data in the negative value as they capture the single-core recirculating region. The depth-averaged shallow water models HO-SWM and Iber+ predict almost identical velocities whilst GBVC predicts larger values but still underestimating the PIV data. Similar values to the GBVC are found for the LES code, Hydro3D, with smaller U values near the upstream wall of the cavity ($x/l \approx 0$). Results from the OpenFOAM simulations with $k-\omega$ SST turbulence and single phase show negative velocity maxima closer to the upstream end of the cavity which differs from the rest of the models and is independent of the turbulence model used (Figure 7). DualSPHysics features a similar magnitude to the experimental measurements with an agreement in the streamwise location of the largest velocity values. The distribution of the transverse velocity component in profiles at $y/w = 0.40$ is shown in Figure 5d. DualSPHysics achieves a close match to the PIV data over most of the profile length, whilst the GBVC model overpredicts the transverse component at both cavity extremes. Between $0.4 \leq x/l \leq 0.8$, there is a good match from all the other models (Hydro3D, OpenFOAM, HO-SWM, GBVC and Iber+) with the PIV data albeit some differences between them are seen nearer the cavity walls, especially at the downstream one ($x/l = 1.0$). GBVC and Hydro3D develop a very similar profile throughout the longitudinal profile.

Profiles of streamwise velocity at $y/w = 0.60$, presented in Figure 5b, indicate that all numerical models predict a positive value whilst the PIV data is always negative, a consequence of a different prediction of the transverse location of the recirculation's core. OpenFOAM, however, shows negative U values before $x/l = 0.4$. The maximum velocities are predicted by DualSPHysics followed by Hydro3D, whilst these are much reduced in the HO-SWM and GBVC. Hydro3D and Iber+ appears to predict the location of the velocity maximum at $x/l \approx 0.4$ whilst the other models estimate this to be closer to the downstream wall, e.g. maximum in the GBVC model is $x/l \approx 0.7$. Figure 5e shows the results of the transverse velocity component (V) at $y/w = 0.60$. Similarly to those at $y/w = 0.4$, DualSPHysics agrees with the PIV data across the centre of the cavity length, with a slight underestimation nearer the velocity maximum at $x/l \approx 0.3$. The GBVC model shows a similar velocity gradient compared with the PIV in the range covering $0.4 < x/l < 0.8$, although it predicts the largest velocities close to the upstream cavity wall compared to the other computational models. The LES code, Hydro3D, shows a good prediction in the centre of the cavity, especially between $0.5 < x/l < 0.85$. RANS results from OpenFOAM feature a less sharp velocity change across the cavity width, with a velocity overshoot near $x/l = 1.0$ that closely follows Hydro3D and GBVC results. HO-SWM shows a slightly better agreement than OpenFOAM whilst Iber+ predicts lower transverse velocities in the downstream half of the cavity.

Figure 5c presents the distribution of U at $y/w = 0.8$ which is relatively close to the shear layer developed at the cavity mouth (Mignot et al., 2016; Ouro et al., 2020a). The models consistently overestimate the PIV velocities, although it should be noted that post-processing of PIV results might have reduced the actual magnitude of velocities (Juez, Buhlmann, et al., 2018). DualSPHysics and Hydro3D predict streamwise velocities to reach approx 0.05 $\mathrm{m\,s^{-1}}$ at mid-length of the cavity, whilst these reduce by a half in the results of OpenFOAM and HO-SWM. Iber+ and GBVC predict a streamwise velocity distribution similar to that of OpenFOAM but with slightly higher magnitude. In terms of the transverse velocity, shown in Figure 5f, at this transverse location, all computational models notably underestimate the velocity peak at $x/l \approx 0.3$ seen in the PIV data. Over the upstream half of the cavity, Hydro3D, Iber+, GBVC and HO-SWM show a similar distribution and magnitude of velocities, whilst OpenFOAM and DualSPHysics predict lower velocities. Near the downstream end, OpenFOAM, GBVC and Hydro3D feature a maximum negative velocity of about $-0.1\,\mathrm{m\,s^{-1}}$, whilst HO-SWM shows a closer match to the PIV data with V reaching $-0.03\,\mathrm{m\,s^{-1}}$.

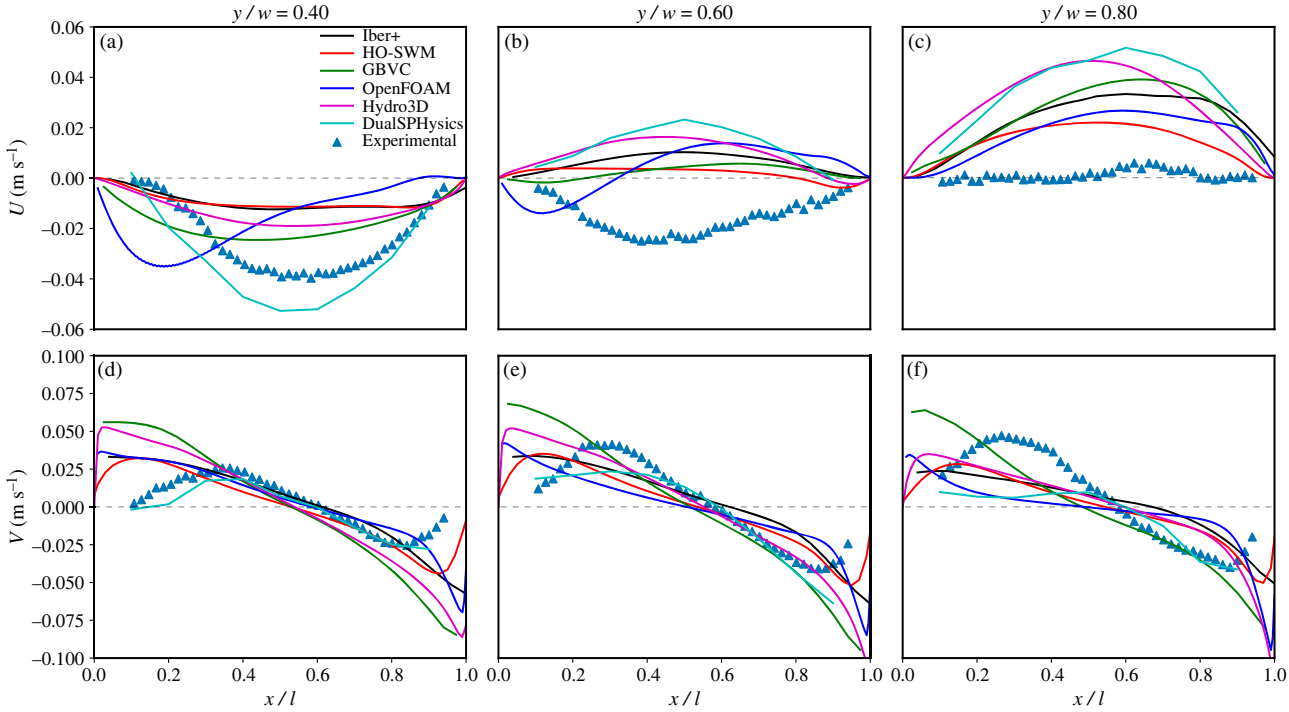

Figure 5. Profiles in x-direction within the lateral cavity of reference at relative locations $y/w = 0.4$ (left), 0.6 (middle) and 0.8 (right) of streamwise (top) and transverse (bottom) velocities. Results correspond to benchmark 1 including PIV data from experiments and the six numerical models tested.

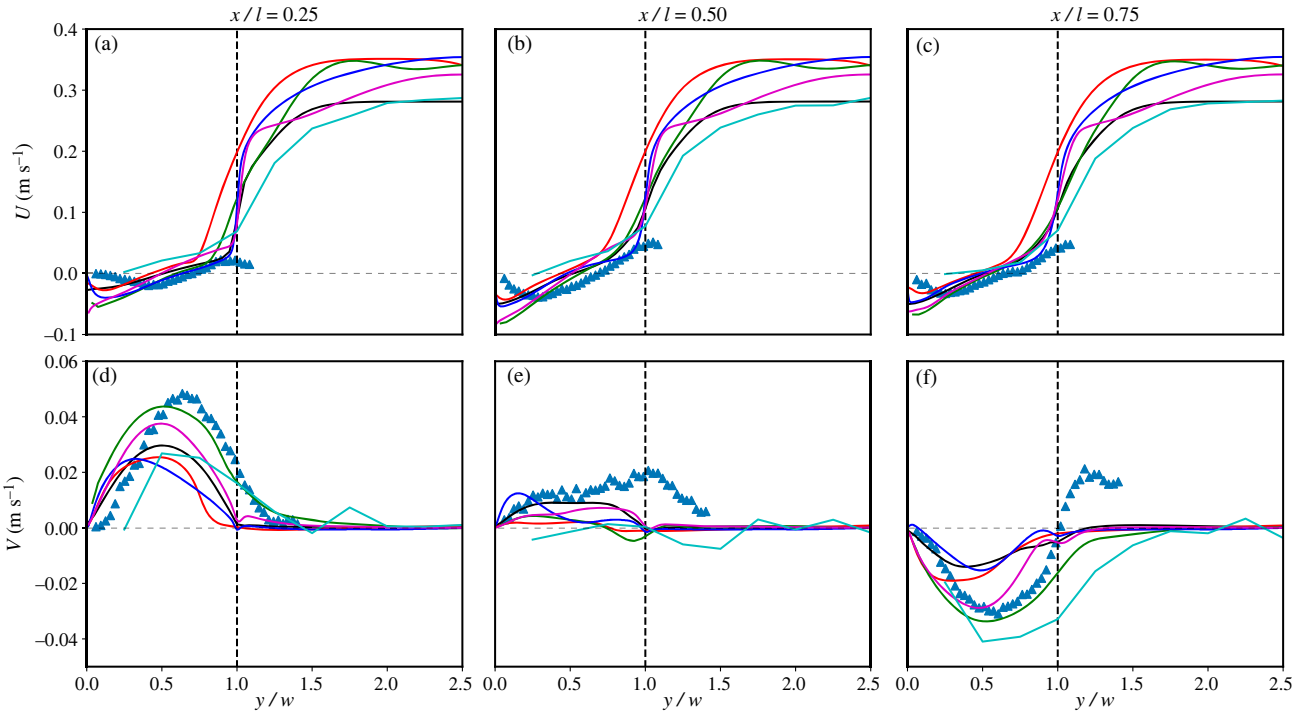

Figure 6. Profiles in y-direction at relative locations $x/l = 0.25$ (left), 0.50 (middle) and 0.75 (right) of streamwise (top) and transverse (bottom) velocities. Results correspond to benchmark 1 including PIV data from experiments and the six numerical models tested. Same legend as Figure 5.

The latter is similar to DualSPHysics which features a good agreement with the PIV data.

Transverse profiles at three downstream stations, $x/l = 0.25, 0.50$ and 0.75, are presented in Figure 6 for the PIV data and all computational models covering half of the entire channel ($y/w = 2.5$). These transverse profiles capture the transition from the main channel to the in-cavity flow, thus inform how the shear layer, over which momentum is exchanged, is captured. At $x/l = 0.25$, Figure 6a, it is seen that the flow field predicted by the computational models differs notably. The shallow-water models HO-SWM and GBVC feature

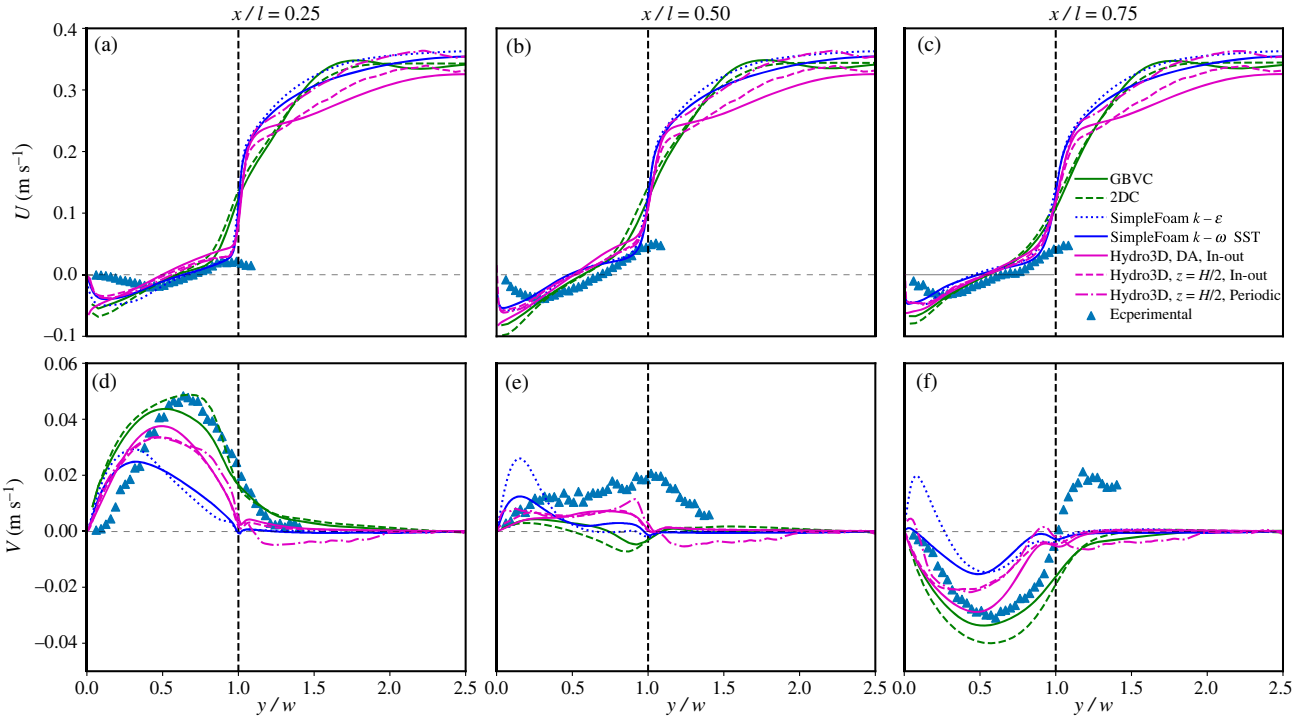

Figure 7. Profiles in y-direction within the lateral cavity of reference at relative locations $x/l = 0.25$ (left), 0.50 (middle) and 0.75 (right) of streamwise (top) and transverse (bottom) velocities. Results correspond to benchmark 1 including PIV data from experiments and the six numerical models tested.

a similar velocity gradient in the shear layer region although its onset location differs, and achieve velocities of about 0.35 m s^{-1} in the middle of the main channel, which is similar to the OpenFOAM results with the difference that the latter has a sharper shear layer transition and good match with the PIV within the cavity. This shear layer prediction is very similar to that of Hydro3D, which estimates slightly lower velocities in the middle of the channel of about 0.32 m s^{-1} which remain higher than the mean bulk velocity (U_0) is 0.295 m s^{-1}. Iber+ reaches bulk velocity after $y/w >$ 1.75, and shows a similar sharp shear-layer to the three-dimensional models Hydro3D and OpenFOAM. The particle-based DualSPHysics exhibits streamwise velocities very close to the bulk velocity in the centre of the channel, predicting a wider shear layer transition. Figure 6d presents the distribution of V at the same profile at $x/l = 0.25$. GBVC yields a very good match to the PIV velocities, especially in the shear-layer region ($y/w \approx 1.0$). Hydro3D captures the transverse velocity increase within the cavity with a similar distribution to Iber+, but with the latter showing lower velocity magnitude. HO-SWM seems to estimate the shear-layer to occur at inner position than the other models, whilst DualSPHysics estimates a wider shear layer compared to the other models. OpenFOAM is able to capture the channel-cavity transition with a V maximum skewed to the lower part of the cavity compared to the PIV results.

Predictions in the main channel at $x/l = 0.50$ and 0.75 (Figure 6b,c) are very similar to those at $x/l =$ 0.25, with some differences between numerical models observed within the cavity. All models improve their results at $x/l = 0.75$ compared to the PIV data, whilst overestimating the experiments at $x/l = 0.50$. Further differences between models are observed in the transverse velocity (V) distribution at these transverse profiles. Figure 6f exhibits large differences between the PIV velocities and the computed results, especially for $y/w > 0.5$ with only the GBVC model providing a close match. At $x/l = 0.75$, the negative transverse velocities, which originate from the flow entraining the cavity over the downstream wall, are somewhat captured by the models. DualSPHysics overpredicts V values and also extent of the shear layer. Hydro3D shows a close agreement with PIV albeit there is an underprediction of velocities between $0.5 < y/w <$ 1.0. HO-SWM, OpenFOAM and Iber+ show the lowest transverse velocity values, perhaps a result of the numerical dissipation introduced by RANS turbulence models.

Sensitivity to the numerical setup or turbulence model adopted in GBVC, OpenFOAM and Hydro3D is further analysed for this benchmark in Figure 7, with comparison of various setup options. Results show that OpenFOAM's prediction with a $k-\varepsilon$ or $k-\omega$ SST model does not vary significantly, with the former yielding slightly larger U velocities in the centre of the channel and V velocities near the wall at $y/w = 0$. Comparing 2DC and GBVC, again there are no truly relevant differences, with some seen in the peak magnitude of the transverse velocity profiles. However, for Hydro3D there are some differences between the

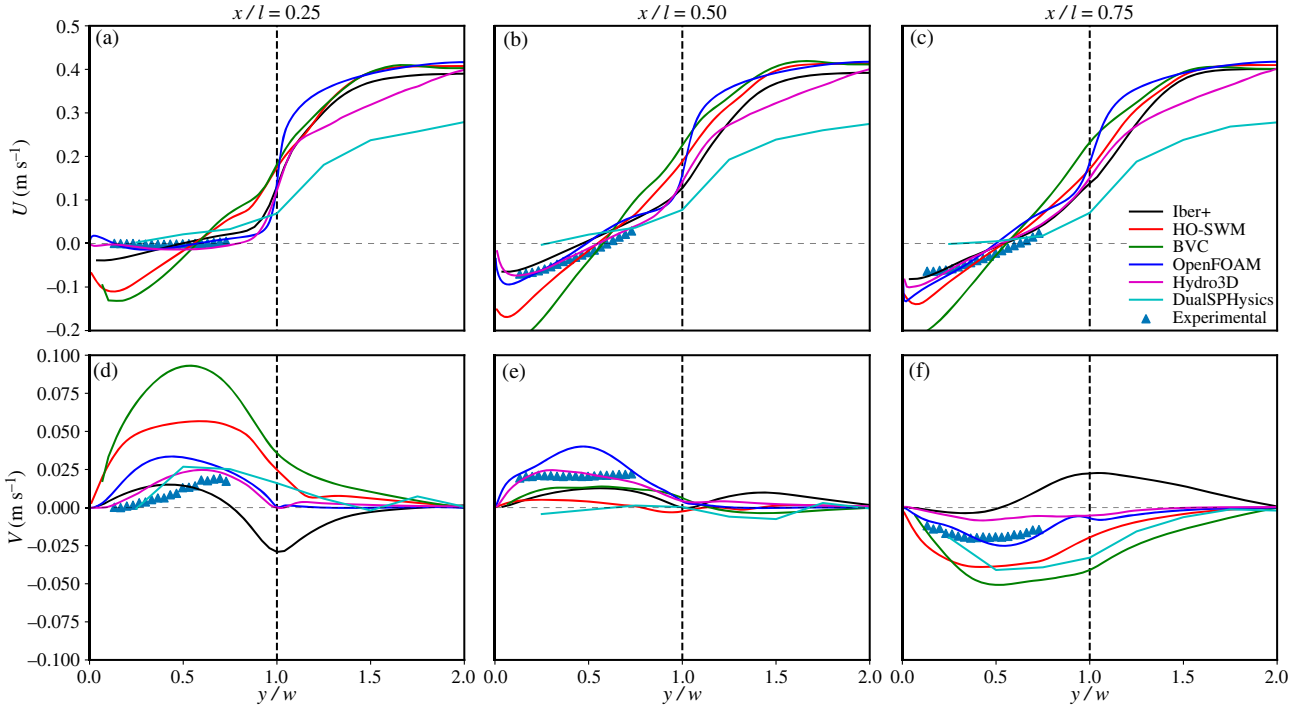

Figure 8. Profiles in y-direction at relative locations $x/l = 0.25$ (left), 0.50 (middle) and 0.75 (right) of streamwise (top) and transverse (bottom) velocities. Results correspond to benchmark 2 including PIV data from experiments and the six numerical models tested.

simulations using a long domain (with identical dimensions to the experimental flume) with inflow-outflow conditions or a shorter domain with periodic conditions and three lateral cavities on each side. The use of periodic conditions leads to larger velocities in the centre of the channel, as the flow reaches a fully developed state that might not be present in the experiment and inflow-outflow computation. Comparing depth-averaged (DA) velocities to those at mid-depth also show significant differences near the centre of the channel, with higher velocities for those at half water depth.

4.2. Benchmark 2

Results of time-averaged streamwise and transverse velocities over profiles at the same relative locations as benchmark 1 (shown in Figure 4) for benchmark 2 are provided here.

The transverse profiles at $x/l = 0.25, 0.50$ and 0.75 are shown in Figure 8. The relatively small velocities over the upstream part at x/l shown in the PIV data is in agreement with results mainly from OpenFOAM, Hydro3D and Iber+, whilst HO-SWM and GBVC predict larger (negative) in-cavity streamwise velocity. Results from DualSPHysics underestimate PIV velocities along the cavity. The latter three models also show a wider shear layer until the main-channel velocity is reached at about $y/w = 1.5$. The mean channel velocity of approx. 0.4 m s^{-1} predicted by the HO-SWM and GBVC agree well with OpenFOAM and Iber+ albeit these estimate a much sharper transition from the cavity to the main channel. This thin shear layer found in OpenFOAM is similar to that predicted by Hydro3D, which estimates smaller velocities in most of the main channel. Depth-averaged values from DualSPHysics also feature lower velocities in the main channel compared to the other models. In terms of the transverse velocity at this profile location, shown in Figure 8d, Hydro3D provides the closest match to the PIV data, with DualSPHysics also showing comparable velocity magnitudes. OpenFOAM resolves larger velocities whilst Iber+ shows a velocity drop between $0.6 < y/w < 1.0$. The other two shallow-water models exhibit larger V values, likely due to estimating a stronger recirculation.

At the middle of the cavity, the profile at $x/l = 0.50$ shows a very similar velocity distribution for most models when compared to PIV and in the main channel location, with the GBVC model predicting larger negative streamwise velocities closer to the cavity's wall. Analogous results are shown in Figure 8c at $x/l = 0.75$, with a slightly smaller velocity gradient over the shear layer. The transverse velocity at $x/l = 0.50$ shows and Hydro3D follows closely the PIV data, with Iber+ and GBVC showing reduced velocities but similar pattern and with OpenFOAM being the only model that overestimates this velocity component. HO-SWM and DualSPHysics features mostly zero values at this location. Nearer the cavity's end at $x/l = 0.75$, OpenFOAM agrees well with PIV data in magnitude and spatial distribution, whereas Iber+ and Hydro3D underestimated the experimental results. GBVC, DualSPHysics and HO-SWM show larger negative velocities both in the cavity region and main channel.

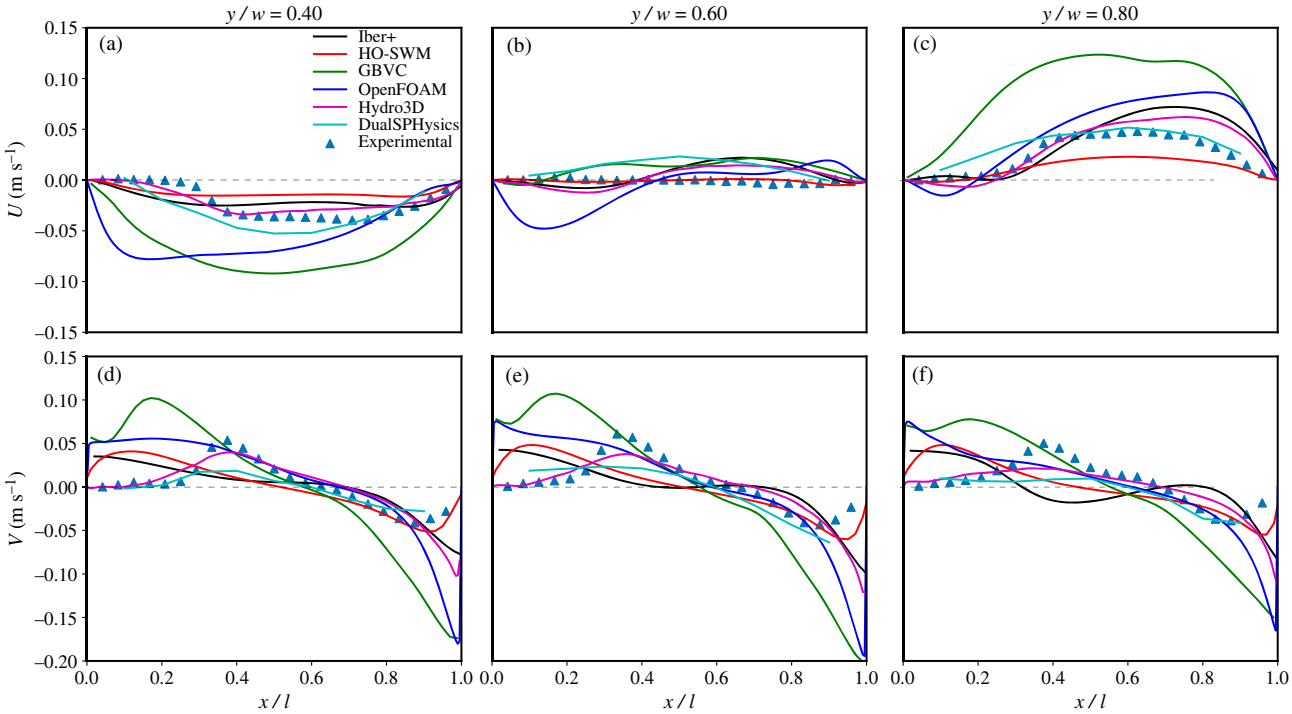

Figure 9. Profiles in x-direction within the lateral cavity of reference at relative locations $y/w = 0.4$ (left), 0.6 (middle) and 0.8 (right) of streamwise (top) and transverse (bottom) velocities. Results correspond to benchmark 2 including PIV data from experiments and the six numerical models tested.

The in-cavity flow is further compared in Figure 9 with profiles at $y/w = 0.4, 0.6$ and 0.8 which span the entire cavity length ($0 \leq x/l \leq 1$). The profiles of streamwise velocity show that the GBVC method predicts a stronger recirculation resulting in larger negative velocities at $y/w = 0.4$ and positive velocities at $y/w = 0.8$, which is similar to the results from OpenFOAM, whose results show reduced values. Hydro3D shows a good match with PIV except at $y/w = 0.4$ between $0.4 < x/l < 0.9$ where it underestimates the PIV data. The depth-averaged shallow-water models HO-SWM and Iber+ feature reduced velocity values at most profiles, perhaps a result of an excessive numerical dissipation. DualSPHysics shows a very good agreement with the PIV velocities for most longitudinal profiles shown in Figure 9, except at $y/w = 0.6$, likely a result of predicting a different location of the recirculation region.

Analogous profile locations for V, Figure 9d–f, indicate again that GBVC and OpenFOAM tend to predict large velocities near the cavity walls whilst their prediction in the central region of the cavity agrees well with the PIV data. HO-SWM shows a slight transverse velocity overprediction in the uppermost wall but it captures the experimental data in the downstream half of the cavity quite well. Similar V distribution is found in the results from Iber+ but with a poorer agreement with the experiments. Hydro3D captures the velocity distribution at the three longitudinal profiles, especially regarding the location of the maximum at $x/l \approx 0.4$ followed by a progressive decay. Similarly, DualSPHysics captures the transverse velocity distribution except near $x/l = 0.4$ as the velocity peak is not captured.

The transient phenomenon of lateral seiching is developed in this lateral cavity benchmark geometry as a result of the cavities leading to a shedding frequency of the shear-layer vortical structures close to that of the natural standing wave of the open channel. The theoretical natural resonant frequency of the open channel is $f = (gh)^{0.5}/2B$, with g denoting gravity acceleration, equal to 0.35 Hz. Only in benchmark 2 a standing wave was observed during the experiments and not in benchmark 1. At two selected locations P1 (within the cavity) and P3 (centre of the main channel), shown in Figure 3, time series of water elevation from the shallow water models (GBVC, HO-SWM) and two-phase OpenFOAM simulation, and of pressure fluctuations from Hydro3D (where a rigid-lid is adopted for representing the free surface) are used to determine whether each numerical model is able to capture this hydrostatic effect for the benchmark 2 setup. The time series are processed with the pwelch function to generate the power spectral density in which spectral energy peaks would depict the frequencies dominating the free-surface oscillation. Note that at P3, there is a standing wave node for the first harmonic due to channel symmetry and the governing frequency doubles as a harmonic should be captured at this location. Figure 10 presents the spectra of the four numerical models compared to that of the experiments (water elevation measurements) and including the theoretical frequency of 0.35 Hz and its first harmonic at 0.70 Hz. Experimental data show the largest peak near the expected frequency but slightly overpredicting this at P1 and underestimating it at P3. At both points, P1 and P3, the shallow-water

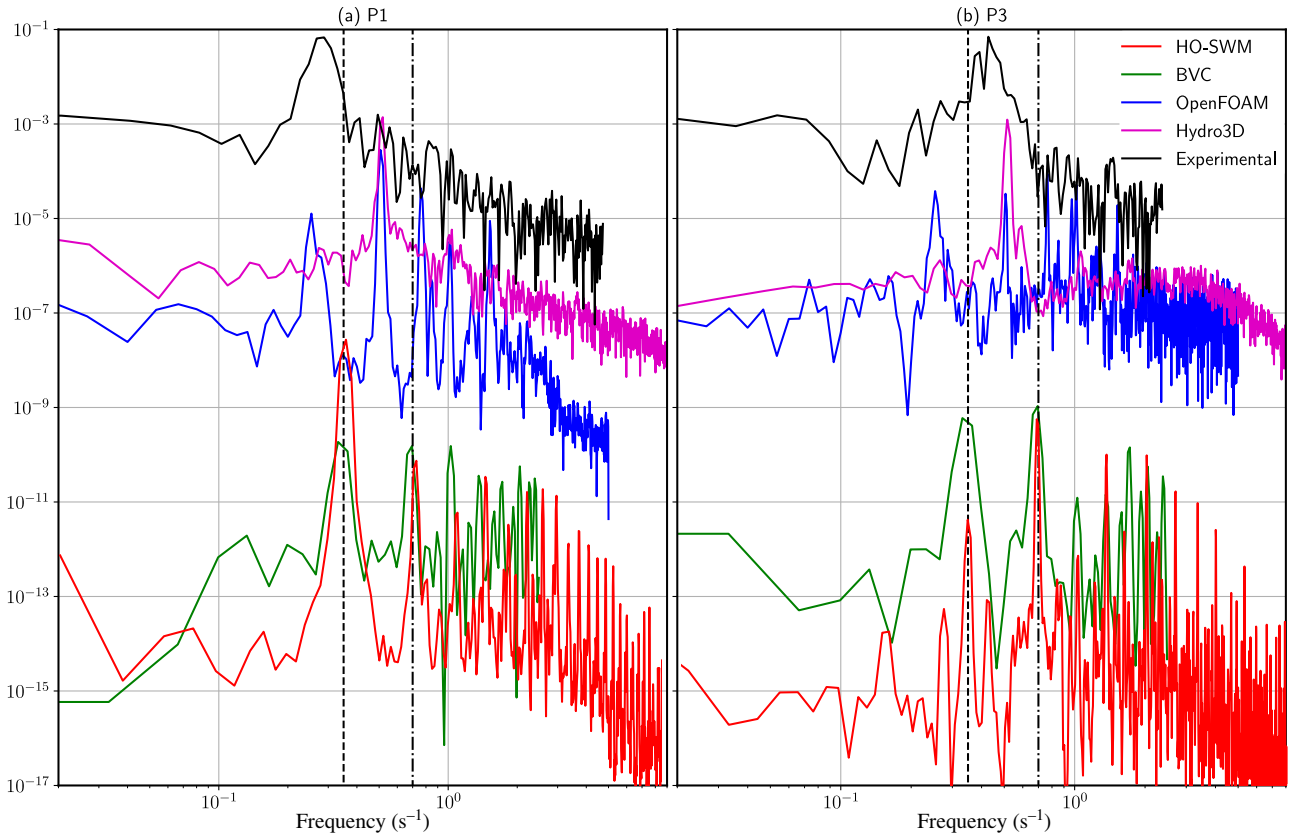

Figure 10. Power spectral density (PSD) computed from time series of transverse velocity fluctuation (v') at points P1 (inside the cavity) and P3 (middle of the main channel) from the HO-SWM, GBVC, OpenFOAM and Hydro3D models. Dashed line corresponds to the natural resonant frequency of 0.35 Hz and the dash-dot line is at its first harmonic. Spectral content (y-axis) of some spectra has been reduced to enable comparison.

models HO-SWM and GBVC capture the standing wave frequency very well, agreeing in the presence of secondary energy peaks at the first harmonic of the resonant frequency. However, these models cannot capture the energy cascade due to the absence of turbulence resolution. At P1, located within the cavity, the three-dimensional models (Hydro3D and OpenFOAM) predict the largest spectral content to be at a frequency of 0.51 Hz. OpenFOAM's spectrum also exhibits harmonics of this frequency and another peak at 0.25 Hz, and fails to capture the turbulence energy cascade due to the time-averaging data of RANS. Note that in OpenFOAM only half of the channel width is modelled. In the LES of Hydro3D the energy cascade is well captured after a frequency of approximately 5 Hz, preceded with a slight energy increase in the 1–5 Hz range at P3. In the middle of the channel, at P3, a secondary peak at 1 Hz is predicted by OpenFOAM, Hydro3D and GBVC, whilst the spectrum of HO-SWM exhibits the largest spectral energy content at the second-harmonic frequency.

5. Discussion of the computational expense and lessons learnt

To evaluate the performance of the computational hydraulics models, different aspects of their computational complexity are evaluated to determine the trade-off between physics accuracy and computational cost. In Figure 11 the computational cost in terms of PUhours (processing unit hours to acknowledge differences in CPU – cores – and GPU – threads) of benchmark 1 simulations is provided in semi-log scale. Despite the complexity of comparing six codes that ran on different environments (e.g. different clusters and compilers) this figure clearly shows the exponential increase in computational cost relative to the model used. Notably, the LES with Hydro3D are in the order of 10^5 PU hours, an order of magnitude larger than DualSPHysics and URANS in OpenFOAM. The shallow-water models span from 10^3 PU hours of HO-SWM, which adopts high-order scheme that are more computationally demanding than those in Iber+ and thus the very low computational cost of the latter.

Whilst this comparison is, to the authors' best knowledge, the most extensive, direct comparison between numerical frameworks, a deeper analysis of their performance is required. For instance, in these benchmarks, contributors did not have a target physical time to simulate and computational cost is not a measure that informs the accuracy of the model as such. Tables 4 and 5 specify the grid resolution, time integration (variable or fixed time step), total number of grid cells, processing units (PUs), computational time, physical time simulated, and relative measures of PUhours

Table 4. Details of the numerical setup, total number of grid cells, number of processing units (PUs), and computational and physical time of the different models. Order is from smallest to largest grid size.

Code	Details	Δx or d_p	Time integration	Number cells	PUs	Compute time	Physical time
Hydro3D	In–Out	0.001 m	CFL = 0.30	300M	600 CPU	336 h	333 s
	Periodic	0.001 m	CFL = 0.30	55M	100 CPU	336 h	578 s
OpenFOAM	Rigid-lid	0.003 m	CFL = 0.45	1.2M	120 CPU	36 h	3000 s
DualSPhysics	SPH	0.005 m	CFL = 0.20	3.0M	3500 GPU th	3.02 h	50 s
HO-SWM	–	0.005 m	CFL = 0.45	310k	24 OMP th	48 h	300 s
BVC	2DC	0.010 m	$\Delta t = 0.2$ s	75k	1 CPU	56.5 h	640 s
	GBVC	0.010 m	$\Delta t = 0.2$ s	75k	1 CPU	79.5 h	640 s
Iber+	GPU	0.010 m	CFL = 0.45	123k	2304 GPU th	0.03 h	300 s
	CPU	0.010 m	CFL = 0.45	123k	1 CPU	3.5 h	300 s

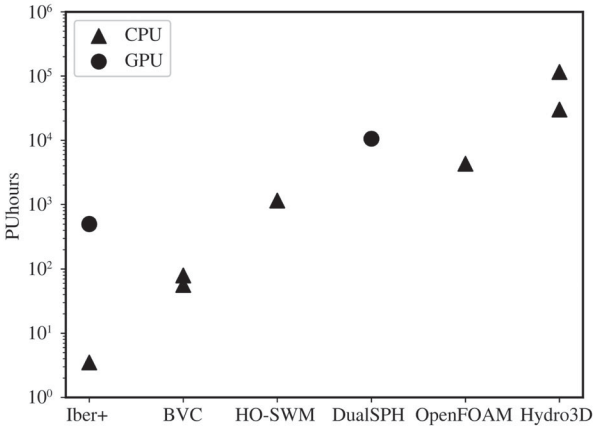

Figure 11. Computational cost obtained for each code to resolve the benchmark 1 with PUhour values in logarithmic scale, with triangles denoting CPU-computed and circles GPU-computed simulations.

Table 5. Comparison of relative computational and physical times with number of cells used by the different numerical models.

Code	Details	PUhours/number cells	Compute/physical time	PUhours/number cells (10^3)/physical time
Hydro3D	In–Out	0.384	346.3	1.15
	Periodic	0.548	52.1	0.95
OpenFOAM	RANS	3.600	1.44	1.20
DualSPhysics	SPH	3.523	211.4	70.47
HO-SWM	–	3.716	3.84	12.39
BVC	2DC	0.753	0.09	1.18
	GBVC	1.060	0.12	1.66
Iber+	GPU	4.059	1.664	13.53
	CPU	0.028	0.011	0.09

per number of cells, computational time over physical time, and PUhours per number of cells and physical time simulated. Iber+ manages to run 300 s of physical time only in 120 s. LES is the most time-consuming model as it adopts the highest resolution of 0.001 m, that is 1000 times more elements than Iber+ or GBVC, or 125 times those used in HO-SWM. Thus, the relative measure of PUhours per total number of cells in Table 5, indicates that Hydro3D is actually very efficient when compared to the other models. This measure increases for OpenFOAM, which is a finite volume code and thus expected to be slower than the finite-differences-based Hydro3D. Comparing computational time against physical time, it is seen that OpenFOAM with rigid lid, GBVC and Iber+ manage to compute faster the run than the output simulated time.

Finally, some reflections on this new benchmark exercise in computational hydraulics are given to give the reader a clearer understanding of the process followed in this activity and to motivate future actions. The main goal was to validate the capability of different numerical models in predicting the complex flow in lateral cavities. The information provided to modellers concerned mostly the experimental setup, flow conditions and what output was sought to be later compared, say profiles of velocities. Hence, no guidance was given as to how boundary conditions needed to be modelled, which led to some modellers simulating two-lateral-cavity open-channel flow with periodic streamwise boundary conditions (Hydro3D), or even further considering half channel width (OpenFOAM), whilst others (mostly shallow-water models, Hydro3D and SPH) simulated the entire channel's dimensions. Physical time to be run and criteria to determine flow variable convergence was up to the modeller. Some ran very long simulations whilst others relatively short. Participants to this benchmark were able to validate their model predictions of time-averaged velocities as the experimental (and some CFD) data were already published. However, there were challenges when comparing how the physics were resolved by each model, e.g. accounting for turbulence statistics or behaviour of instantaneous flow structures, which cannot be provided by steady-state models or those resolving the 2-D flow. Future benchmarks will involve blind tests, which will demand modellers to have a well-defined modelling protocol.

6. Conclusions

This paper presents a first-of-its-kind international computational hydraulics benchmark with application to two open-channel flows with symmetric lateral cavities. Numerical models span from two-dimensional (Iber+ and HO-SWM) and quasi-3D (GBVC) shallow-water models, incompressible Navier–Stokes with RANS (OpenFOAM) and LES (Hydro3D) turbulence closures, and a smoothed particle hydrodynamics code

(DualSPHysics). These were compared with experimental PIV data of streamwise and transverse velocities at six selected profiles normal to and in the direction of the in-channel main flow. All models were able to capture the main flow physics involved, especially the single core recirculation, but differences in the velocity magnitude in the main channel or shear-layer over the cavity mouth were pronounced. The GBVC model showed a close match to the PIV data in benchmark 1 whilst predicted the largest velocities in benchmark 2 likely due to resolving a stronger in-cavity flow. The three-dimensional models, OpenFOAM, DualSPHysics and Hydro3D, predicted sharper velocity gradients at the mouth of the cavity, probably due to the lower numerical dissipation introduced (especially compared to shallow-water models) and resolution of the three-dimensional flow field as they can explicitly account for heterogeneous momentum transfer between the cavities and main channel. Iber+ was the fastest code with results showing a relatively good performance, especially in benchmark 1, similarly to the results from the HO-SWM code, both of which showed an underprediction of velocities in benchmark 2. Resolution of instantaneous flow features by the adopted models was analysed through power spectral density of time series of water elevation or pressure fluctuations (when a rigid lid top boundary condition was used at the free surface) at two selected transverse locations. Shallow-water models captured very well the theoretical hydrostatic standing wave, whilst the three-dimensional models predicted its frequency to happen with a higher value, likely due to a lower capability to account for this free-surface resonance. Further comparison between models requires computation of the Reynolds stresses or instantaneous flow structures to estimate the flow scales that are resolved ; however, this was not possible and it constitutes a challenge when comparing codes of different nature. Finally, the computational cost of each model for the performed simulations was quantified, with results showing an logarithmic growth in computational expense with CPUs with increasing model complexity.

Disclosure statement

No potential conflict of interest was reported by the author(s).

Funding

Dr Ouro gratefully acknowledges the help of the Supercomputing Wales project, which is partially sponsored by the European Regional Development Fund (ERDF) via the Welsh Government. Some of the presented material has been supported by the Dame Kathleen Ollerenshaw Fellowship that Dr Ouro holds at the University of Manchester. Dr Navas-Montilla acknowledges the support of the Regional Government of Aragón (Computational Fluid Mechanics Group, T32_20R). Dr Juez was funded by the ERC-StG 2021 programme of the European union under grant agreement number 101039181-SEDAHEAD and by the Regional Government of Aragón (Geoenvironmental Processes and Global Change group, E02_23R). Dr García-Feal was supported by the postdoctoral fellowship 'Juan de la Cierva' (ref. JDC2022-048667-I), funded by MCIN/AEI/10.13039/50 1100011033 and the European Union 'NextGenerationEU'/PRTR; by the Spanish Ministerio de Universidades under application 33.50.460A.752, by the European Union NextGenerationEU/PRTR through a contract Margarita Salas from the University of Vigo. Dr Croquer acknowledges Prof. Sébastien Poncet as well as the support of the SciNet HPC Consortium. SciNet is funded by Innovation, Science and Economic Development Canada, the Digital Research Alliance of Canada, the Ontario Research Fund: Research Excellence, and the University of Toronto.

Notation

B	channel width (m)
b	width of the base channel (m)
d_p	interparticle distance (m)
f	frequency (s^{-1})
g	gravity acceleration depth ($m\,s^{-2}$)
h	water depth (m)
k_s	equivalent roughness (m)
L	distance between two cavities (m)
l	length of the cavities (m)
Q	flow rate ($m^3\,s^{-1}$)
T	period (s)
u	velocity ($m\,s^{-1}$)
u_b	velocity at the bottom surface ($m\,s^{-1}$)
u_s	velocity at the water surface ($m\,s^{-1}$)
U	depth-averaged velocity at the water surface ($m\,s^{-1}$)
U_0	bulk velocity ($m\,s^{-1}$)
w	cavity width (m)
x	streamwise direction coordinate (m)
z	vertical direction coordinate (m)
z_s	water surface elevation (m)
z^+	vertical grid size in wall units (−)
β	empirical coefficient for the horizontal component of the turbulent viscosity (−)
Δt	time step (s)
Δx	grid cell size (m)
η	normalized water elevation (−)
λ	empirical coefficient for the vertical component of the turbulent viscosity (−)

ORCID

Pablo Ouro http://orcid.org/0000-0001-6411-8241
Luis Cea http://orcid.org/0000-0002-3920-0478
Sergio Croquer http://orcid.org/0000-0001-6870-3050
Orlando Garcia-Feal http://orcid.org/0000-0001-6237-660X
Adrián Navas-Montilla http://orcid.org/0000-0002-3465-6898
Benedict D. Rogers https://orcid.org/0000-0002-3269-7979
Tatsuhiko Uchida http://orcid.org/0000-0003-3130-1175
Carmelo Juez http://orcid.org/0000-0002-2985-1023

References

Barros, M., & Escauriaza, C. (2024). Lagrangian and Eulerian perspectives of turbulent transport mechanisms in a lateral cavity. *Journal of Fluid Mechanics*, *984*, A1. https://doi.org/10.1017/jfm.2024.99

Bladé, E., Cea, L., Corestein, G., Escolano, E., Puertas, J., Vázquez-Cendón, M. E., Dolz, J., & Coll, A. (2014). Iber: Herramienta de simulación numérica del flujo en ríos. *Revista Internacional de Métodos Numéricos para Cálculo y Diseño en Ingeniería*, *30*(1), 1–10.

Bomminayuni, S., & Stoesser, T. (2011). Turbulence statistics in an open-channel flow over a rough bed. *Journal of Hydraulic Engineering*, *137*(11), 1347–1358. https://doi.org/10.1061/(ASCE)HY.1943-7900.0000454

Castro-Orgaz, O., Hager, W. H., & Katopodes, N. D. (2023). Variational models for nonhydrostatic free-surface flow: A unified outlook to maritime and open-channel hydraulics developments. *Journal of Hydraulic Engineering*, *149*(7), Article 04023014. https://doi.org/10.1061/JHEND8.HYENG-13338

Cea, L., Álvarez, M., & Puertas, J. (2022). Estimation of flood-exposed population in data-scarce regions combining satellite imagery and high resolution hydrological-hydraulic modelling: A case study in the Licungo basin (Mozambique). *Journal of Hydrology: Regional Studies*, *44*, Article 101247.

Cea, L., & Bladé, E. (2015). A simple and efficient unstructured finite volume scheme for solving the shallow water equations in overland flow applications. *Water Resources Research*, *51*(7), 5464–5486. https://doi.org/10.1002/wrcr.v51.7

Cea, L., & López-Núñez, A. (2021). Extension of the two-component pressure approach for modeling mixed free-surface-pressurized flows with the two-dimensional shallow water equations. *International Journal for Numerical Methods in Fluids*, *93*(3), 628–652. https://doi.org/10.1002/fld.v93.3

Cea, L., Puertas, J., & Vázquez-Cendón, M. E. (2007). Depth averaged modelling of turbulent shallow water flow with wet–dry fronts. *Archives of Computational Methods in Engineering*, *14*(3), 303–341. https://doi.org/10.1007/s11831-007-9009-3

Cea, L., & Vázquez-Cendón, M. E. (2012). Unstructured finite volume discretisation of bed friction and convective flux in solute transport models linked to the shallow water equations. *Journal of Computational Physics*, *231*(8), 3317–3339. https://doi.org/10.1016/j.jcp.2012.01.007

Cea, L., Vila, G., Garcia-Alen, G., Puertas, J., & Pena, L. (2022). Hydraulic modeling of bridges in two-dimensional shallow water models. *Journal of Hydraulic Engineering*, *148*(8), Article 06022006. https://doi.org/10.1061/(ASCE)HY.1943-7900.0001992

Cercos-Pita, J. L. (2015). AQUAgpusph, a new free 3D SPH solver accelerated with OpenCL. *Computer Physics Communications*, *192*, 295–312. https://doi.org/10.1016/j.cpc.2015.01.026

Constantinescu, G. (2006). LE of shallow mixing interfaces: A review. *Environmental Fluid Mechanics*, *14*(5), 971–996. https://doi.org/10.1007/s10652-013-9303-6

Dalrymple, R. A., & Rogers, B. D. (2006). Numerical modeling of water waves with the SPH method. *Coastal Engineering*, *53*(2–3), 141–147. https://doi.org/10.1016/j.coastaleng.2005.10.004

Darwish, M., & Moukalled, F. (2016). *The finite volume method in computational fluid dynamics: An advanced introduction with OpenFOAM® and Matlab®*. Springer.

Dazzi, S., Vacondio, R., & Mignosa, P. (2020). Internal boundary conditions for a GPU-accelerated 2D shallow water model: Implementation and applications. *Advances in Water Resources*, *137*, Article 103525. https://doi.org/10.1016/j.advwatres.2020.103525

Dewals, B., Bruwier, M., Pirotton, M., Erpicum, S., & Archambeau, P. (2021). Porosity models for large-scale urban flood modelling: A review. *Water*, *13*(7), Article 960. https://doi.org/10.3390/w13070960

Domínguez, J. M., Fourtakas, G., Altomare, C., Canelas, R. B., Tafuni, A., García-Feal, O., Martínez-Estévez, I., Mokos, A., Vacondio, R., Crespo, A. J. C., Rogers, B. D., Stansby, P. K., & Gómez-Gesteira, M. (2022). DualSPHysics: From fluid dynamics to multiphysics problems. *Computational Particle Mechanics*, *9*(5), 867–895. https://doi.org/10.1007/s40571-021-00404-2

Engelen, L., Perrot-Mignot, E., Mignot, E., Riviere, N., & Mulder de, T. (2021). Lagrangian study of the particle transport past a lateral, open-channel cavity. *Physics of Fluids*, *33*(1), 013303. https://doi.org/10.1063/5.0030922

Fourtakas, G., Domínguez, J. M., Vacondio, R., & Rogers, B. D. (2019). Local uniform stencil (LUST) boundary condition for arbitrary 3-D boundaries in parallel smoothed particle hydrodynamics (SPH) models. *Computers and Fluids*, *190*, 346–361. https://doi.org/10.1016/j.compfluid.2019.06.009

Gamero, P., Cantero-Chinchilla, F. N., Bergillos, R. J., Castro-Orgaz, O., & Dey, S. (2022). Shallow-water lee-side waves at obstacles: Experimental characterization and turbulent non-hydrostatic modeling using weighted-averaged residual equations. *Environmental Modelling and Software*, *155*, Article 105422. https://doi.org/10.1016/j.envsoft.2022.105422

García-Feal, O., González-Cao, J., Gómez-Gesteira, M., Cea, L., Domínguez, J. M., & Formella, A. (2018). An accelerated tool for flood modelling based on Iber. *Water*, *10*(10), Article 1459. https://doi.org/10.3390/w10101459

Gotoh, H., & Khayyer, A. (2018). On the state-of-the-art of particle methods for coastal and ocean engineering. *Coastal Engineering Journal*, *60*(1), 79–103. https://doi.org/10.1080/21664250.2018.1436243

Guillén Ludeña, S., Cheng, Z., Constantinescu, G., & Franca, M. J. (2017). Hydrodynamics of mountain-river confluences and its relationship to sediment transport. *Journal of Geophysical Research: Earth Surface*, *122*(4), 901–924. https://doi.org/10.1002/jgrf.v122.4

Guinot, V., Sanders, B. F., & Schubert, J. E. (2017). Dual integral porosity shallow water model for urban flood modelling. *Advances in Water Resources*, *103*, 16–31. https://doi.org/10.1016/j.advwatres.2017.02.009

Hérault, A., Bilotta, G., & Dalrymple, R. A. (2010). SPH on GPU with CUDA. *Journal of Hydraulic Research*, *48*(sup1), 74–79. https://doi.org/10.1080/00221686.2010.9641247

Henonin, J., Hongtao, M. A., Zheng-Yu, Y., Hartnack, J., Havnø, K., Gourbesville, P., & Mark, O. (2015). Citywide multi-grid urban flood modelling: The July 2012 flood in Beijing. *Urban Water Journal*, *12*(1), 52–66. https://doi.org/10.1080/1573062X.2013.851710

Juez, C., Buhlmann, I., Maechler, G., Schleiss, A. J., & Franca, M. J. (2018). Transport of suspended sediments under the influence of bank macro-roughness. *Earth Surface Processes and Landforms*, *43*(1), 271–284. https://doi.org/10.1002/esp.v43.1

Juez, C., Lacasta, A., Murillo, J., & García-Navarro, P. (2022). An efficient GPU implementation for a faster simulation of unsteady bed-load transport. *Journal of Hydraulic*

Research, *54*, 275–288. https://doi.org/10.1080/00221686.2016.1143042

Juez, C., & Navas-Montilla, A. (2022). Numerical characterization of seiche waves energy potential in river bank lateral embayments. *Renewable Energy*, *186*, 143–156. https://doi.org/10.1016/j.renene.2021.12.125

Juez, C., Thalmann, M., Schleiss, A. J., & Franca, M. J. (2018). Morphological resilience to flow fluctuations of fine sediment deposits in bank lateral cavities. *Advances in Water Resources*, *115*, 44–59. https://doi.org/10.1016/j.advwatres.2018.03.004

Kalita, H. M., Das, R., Hajong, A., Kumar, N., Kharnaior, D., & Dkhar, H. C. (2019). Experimental and numerical flow simulation over weirs. *Water Resources*, *46*(6), 934–943. https://doi.org/10.1134/S0097807819060083

Khosronejad, A., Kang, S., & Sotiropoulos, F. (2012). Experimental and computational investigation of local scour around bridge piers. *Advances in Water Resources*, *37*, 73–85. https://doi.org/10.1016/j.advwatres.2011.09.013

Lacasta, A., Morales-Hernández, M., Brufau, P., & García-Navarro, P. (2018). Application of an adjoint-based optimization procedure for the optimal control of internal boundary conditions in the shallow water equations. *Journal of Hydraulic Research*, *56*(1), 111–123. https://doi.org/10.1080/00221686.2017.1300196

Launder, B. E., & B. I. Sharma (1974). Application of the energy-dissipation model of turbulence to the calculation of flow near a spinning disc. *Letters in Heat and Mass Transfer*, *1*(2), 131–137. https://doi.org/10.1016/0094-4548(74)90150-7

Loken, C., Gruner, D., Groer, L., Peltier, R., Bunn, N., Craig, M., Henriques, T., Dempsey, J., Yu, C. H., Chen, J., & Dursi, L. J. (2010). SciNet: Lessons learned from building a power-efficient top-20 system and data centre. In *Journal of Physics: Conference Series* (Vol. 256, No. 1, p. 012026). IOP Publishing.

Manenti, S., Wang, D., Domínguez, J. M., Li, S., Amicarelli, A., & Albano, R. (2019). SPH modeling of water-related natural hazards. *Water*, *11*(9), Article 1875. https://doi.org/10.3390/w11091875

Maranzoni, A., Dazzi, S., Aureli, F., & Mignosa, P. (2015). Extension and application of the Preissmann slot model to 2D transient mixed flows. *Advances in Water Resources*, *82*, 70–82. https://doi.org/10.1016/j.advwatres.2015.04.010

Menter, F. R. (1994). Two-equation eddy-viscosity turbulence models for engineering applications. *AIAA Journal*, *32*(8), 1598–1605. https://doi.org/10.2514/3.12149

Mignot, E., Cai, W., Launay, G., Riviere, N., & Escauriaza, C. (2016). Coherent turbulent structures at the mixing-interface of a square open-channel lateral cavity. *Physics of Fluids*, *28*(4), Article 045104. https://doi.org/10.1063/1.4945264

Morales-Hernández, M., Sharif, M. B., Gangrade, S., Dullo, T. T., Kao, S.-C., Kalyanapu, A., Ghafoor, S. K., Evans, K. J., Madadi-Kandjani, E., & Hodges, B. R. (2020). High-performance computing in water resources hydrodynamics. *Journal of Hydroinformatics*, *22*(5), 1217–1235. https://doi.org/10.2166/hydro.2020.163

Nadaoka, K., & Yagi, H. (1998). Shallow-water turbulence modeling and horizontal large-eddy computation of river flow. *Journal of Hydraulic Engineering*, *124*(5), 493–500. https://doi.org/10.1061/(ASCE)0733-9429(1998)124:5(493)

Navas-Montilla, A., Juez, C., Franca, M. J., & Murillo, J. (2019). Depth-averaged unsteady RANS simulation of resonant shallow flows in lateral cavities using augmented WENO-ADER schemes. *Journal of Computational Physics*, *395*, 511–536. https://doi.org/10.1016/j.jcp.2019.06.037

Navas-Montilla, A., Martínez-Aranda, S., Lozano, A., García-Palacín, I., & García-Navarro, P. (2021). 2D experiments and numerical simulation of the oscillatory shallow flow in an open channel lateral cavity. *Advances in Water Resources*, *148*, Article 103836. https://doi.org/10.1016/j.advwatres.2020.103836

Ouro, P., Fraga, B., Lopez-Novoa, U., & Stoesser, T. (2019). Scalability of an Eulerian–Lagrangian large-eddy simulation solver with hybrid MPI/OpenMP parallelisation. *Computers & Fluids*, *179*, 123–136. https://doi.org/10.1016/j.compfluid.2018.10.013

Ouro, P., Juez, C., & Franca, M. J. (2020a). Drivers for mass and momentum exchange between the main channel and river bank lateral cavities. *Advances in Water Resources*, *137*, Article 103511. https://doi.org/10.1016/j.advwatres.2020.103511

Ouro, P., Juez, C., & Franca, M. J. (2020b). Mass and momentum exchange in lateral bank cavities with increasing aspect ratio using large-eddy simulation. In *Proceedings of the 10th Conference on Fluvial Hydraulics, Delft, Netherlands*.

Ouro, P., Lopez-Novoa, U., & Guest, M. (2021). On the performance of a highly-scalable computational fluid dynamics code on AMD, ARM and Intel processor-based HPC systems. *Computer Physics Communications*, *269*, Article 108105. https://doi.org/10.1016/j.cpc.2021.108105

Ouro, P., Navas-Montilla, A., Franca, M. J., & Juez, C. (2022). Modelling turbulent coherent structures in lateral river cavities using large-eddy simulation and a high-order 2D shallow water model. In *Proceedings of the 39th IAHR World Congress (Granada, 2022)*.

Park, S. H., Jo, Y. B., Ahn, Y., Choi, H. Y., Choi, T. S., Park, S. S., Yoo, H. S., Kim, J. W., & Kim, E. S. (2020). Development of multi-GPU-based smoothed particle hydrodynamics code for nuclear thermal hydraulics and safety: Potential and challenges. *Frontiers in Energy Research*, *8*, Article 86. https://doi.org/10.3389/fenrg.2020.00086

Ponce, M., Van Zon, R., Northrup, S., Gruner, D., Chen, J., Ertinaz, F., Fedoseev, A., Groer, L., Mao, F., Mundim, B. C., & Nolta, M. (2019). Deploying a top-100 supercomputer for large parallel workloads: The Niagara supercomputer. In *Proceedings of the Practice and Experience in Advanced Research Computing on Rise of the Machines (Learning)* (pp. 1–8).

Posa, A., & Broglia, R. (2021). Characterization of the turbulent wake of an axial-flow hydrokinetic turbine via large-eddy simulation. *Computers and Fluids*, *216*, Article 104815. https://doi.org/10.1016/j.compfluid.2020.104815

Rastogi, A. K., & Rodi, W. (1978). Prediction of heat and mass transfer in open channels. *Journal of the Hydraulics Division*, *104*(3), 397–420. https://doi.org/10.1061/JYCEAJ.0004962

Rodi, W. (2017). *Turbulence models and their application in hydraulics: A state-of-the-art review*. CRC Press.

Rodi, W., Constantinescu, G., & Stoesser, T. (2013). *Large-eddy simulation in hydraulics*. CRC Press.

Rogers, B. D., & Dalrymple, R. A. (2005). SPH modeling of breaking waves. In *Proceedings of the 29th International Conference on Coastal Engineering. Lisbon, Portugal.*

Sanders, B. F., & Schubert, J. E. (2019). PRIMo: Parallel raster inundation model. *Advances in Water Resources*, *126*, 79–95. https://doi.org/10.1016/j.advwatres.2019.02.007

Shadloo, M. S., Oger, G., & Le Touzé, D. (2016). Smoothed particle hydrodynamics method for fluid flows, towards

industrial applications: Motivations, current state, and challenges. *Computers and Fluids*, *136*, 11–34. https://doi.org/10.1016/j.compfluid.2016.05.029

Shamkhalchian, A., & De Almeida, G. A. (2021). Upscaling the shallow water equations for fast flood modelling. *Journal of Hydraulic Research*, *59*(5), 739–756. https://doi.org/10.1080/00221686.2020.1818316

Sotiropoulos, F. (2015). Hydraulics in the era of exponentially growing computing power. *Journal of Hydraulic Research*, *53*(5), 547–560. https://doi.org/10.1080/00221686.2015.1119210

Sotiropoulos, F. (2019). Hydraulic engineering in the era of big data and extreme computing: Can computers simulate river turbulence? *Journal of Hydraulic Engineering*, *145*(6), 1–13. https://doi.org/10.1061/(ASCE)HY.1943-7900.0001594

Stoesser, T. (2010). Physically realistic roughness closure scheme to simulate turbulent channel flow over rough beds within the framework of LES. *Journal of Hydraulic Engineering*, *136*(10), 812–819. https://doi.org/10.1061/(ASCE)HY.1943-7900.0000236

Stoesser, T. (2014). Large-eddy simulation in hydraulics: Quo Vadis? *Journal of Hydraulic Research*, *52*(4), 441–452. https://doi.org/10.1080/00221686.2014.944227

Sweet, J., Richter, D. H., & Thain, D. (2018). GPU acceleration of Eulerian–Lagrangian particle-laden turbulent flow simulations. *International Journal of Multiphase Flow*, *99*, 437–445. https://doi.org/10.1016/j.ijmultiphaseflow.2017.11.010

Tafuni, A., Domínguez, J. M., Vacondio, R., & Crespo, A. J. C. (2018). A versatile algorithm for the treatment of open boundary conditions in Smoothed particle hydrodynamics GPU models. *Computer Methods in Applied Mechanics and Engineering*, *342*, 604–624. https://doi.org/10.1016/j.cma.2018.08.004

Toro, E. F. (2001). *Shock-capturing methods for free-surface shallow flows*. Wiley.

Uchida, T., & Fukuoka, S. (2014). Numerical calculation for bed variation in compound-meandering channel using depth integrated model without assumption of shallow water flow. *Advances in Water Resources*, *142*(72), 45–56. https://doi.org/10.1016/j.advwatres.2014.05.002

Uchida, T., & Fukuoka, S. (2019). Quasi-3D two-phase model for dam-break flow over movable bed based on a non-hydrostatic depth-integrated model with a dynamic rough wall law. *Advances in Water Resources*, *129*, 311–327. https://doi.org/10.1016/j.advwatres.2017.09.020

Uchida, T., Fukuoka, S., A. N. Papanicolaou, & Takiris, A. G. (2016). Non-hydrostatic quasi-3D model coupled with dynamic rough wall law for simulating flow over rough bed with submerged boulders. *Journal of Hydraulic Engineering*, *142*(11), Article 04016054. https://doi.org/10.1061/(ASCE)HY.1943-7900.0001198

Uijttewaal, W. (2019). Hydrodynamics of shallow flows: Application to rivers. *Journal of Hydraulic Research*, *52*(2), 157–172. https://doi.org/10.1080/00221686.2014.905505

Violeau, D., & Rogers, B. D. (2016). Smoothed particle hydrodynamics (SPH) for free-surface flows: Past, present and future. *Journal of Hydraulic Research*, *54*(1), 1–26. https://doi.org/10.1080/00221686.2015.1119209

Vowinckel, B., Nikora, V., Kempe, T., & Froehlich, J. (2021). Momentum balance in flows over mobile granular beds: Application of double-averaging methodology to DNS data. *Journal of Hydraulic Research*, *55*(2), 190–207. https://doi.org/10.1080/00221686.2016.1260656

Wang, W., Martin, T., Kamath, A., & Bihs, H. (2020). An improved depth-averaged nonhydrostatic shallow water model with quadratic pressure approximation. *International Journal for Numerical Methods in Fluids*, *92*(8), 803–824. https://doi.org/10.1002/fld.v92.8

Xia, X., Liang, Q., & Ming, X. (2019). A full-scale fluvial flood modelling framework based on a high-performance integrated hydrodynamic modelling system (HiPIMS). *Advances in Water Resources*, *132*, Article 103392. https://doi.org/10.1016/j.advwatres.2019.103392

Zhao, C., Hongwei, F., Ouro, P., Stoesser, T., & Dey, S. (2023). Response of bedload and bedforms to near-bed flow structures. *Journal of Hydraulic Engineering*, *150*(1), Article 04023060. https://doi.org/10.1061/JHEND8.HYENG-13618